Anisotropic Plasmonic Nanostructures for Colorimetric

Sensing

Jingbin Zeng^{a,b}, Yu Zhang^a, Teng Zeng^c, Rashed Aleisa^b, Zhiwei Qiu^a, Yuzhu Chen^a, Jiankun

Huang^a, Dawei Wang^{b*}, Zifeng Yan^a, Yadong Yin^{b*}

^aCollege of Science, China University of Petroleum (East China), Qingdao, 266555(China)

^bDepartment of Chemistry, University of California, Riverside, USA, 92521

^cDepartment of Civil and Environmental Engineering, Syracuse University, 151 Link Hall, Syracuse,

NY 13244, United States

Corresponding authors.

E-mail address: wdwhhu@gmail.com (D.Wang); yadong.yin@ucr.edu (Y.Yin)

Abstract

Colorimetric detection is important for various applications where instant and

convenient read-out is needed. Because of their fascinating optical properties,

plasmonic nanostructures have inspired numerous colorimetric detections for

environmental contaminants, biomolecules, and pharmaceuticals. The underlying

mechanism of these colorimetric sensors is that the introduction of analytes can alter

the distance, spatial arrangement (orientation), size, morphology, or composition of

plasmonic nanostructures, inducing distinguishable changes of spectra and color. In this

review, we focus our discussion on the colorimetric detection involving anisotropic

nanostructures such as nanorods, nanoplates, nanoflowers, nanobipyramids,

nanoframes, and nanocubes, which exhibit many unique advantages compared to their

isotropic counterparts. In addition to illustrating the design principles, sensing

mechanisms, and applications of these anisotropic nanostructures-based colorimetric

methods, we also discuss smart plasmonic sensors based on anisotropic nanomaterials

that are used to detect external stimuli such as temperature, pH, light, magnetic field,

and mechanical force.

Keywords: localized surface plasmon resonance, colorimetric, sensing, detection,

anisotropic nanostructures, shape

1

Introduction	3
Anisotropic plasmonic nanostructures	4
Au nanorods	5
Au nanoplates	6
Au nanobipyramids	6
Au nanoflowers	7
Au nanoframes	7
Au nanocubes	7
Detection mechanisms	9
Change of interparticle distance	9
Aggregation (Random assembly)	9
Oriented assembly (Side-by-side and End-to-end)	16
Morphology, size, and composition change	18
Etching	19
Deposition (growth)	25
Transformation	30
External stimuli	32
Optically responsive materials	33
Magnetically responsive materials	35
Electrically responsive materials	37
Other Stimuli	39
Summary and Outlook	40
References	41

Introduction

Colorimetric assay has been of particular interest for on-the-spot detection of analytes due to its straightforward readout, convenient operation, and minimal requirement for instrumentation. Traditionally, organic chromophores with highly delocalized conjugated systems are employed as colorimetric receptors. However, they often suffer from low sensitivity because of their low molar extinction coefficients (more than 3 orders lower than that of gold or silver nanoparticles). In addition, some chromogenic reactions occur in non-aqueous media, which greatly limit their practical applications. Over the last several decades, plasmonic nanomaterials, such as gold, silver, copper and/or their composites, have been employed for colorimetric sensing of a variety of analytes ranging from chemical warfare agents [1], heavy metals [2-5], anions [6], neurochemicals [7, 8], proteins [9, 10], nucleic acids [11], disease biomarkers [12, 13] to cancer cells [14] etc., due to their distinct optical property of localized surface plasmon resonance (LSPR). LSPR is an optical phenomenon based on oscillating free electrons at the surface of the metals when they interact with incident light, resulting in coherent localized plasmon oscillations with a resonant frequency. Because of this phenomenon, plasmonic nanomaterials usually show strong extinction in the visible region, together with corresponding colors. LSPR is highly dependent on the size, composition, morphology, inter-particle distances, and orientation of plasmonic nanostructures, thus allowing designs of signal transducers for visual readout [15]. Even though some previous review articles have extensively discussed the mechanisms employed in the colorimetric sensors and their wide applications, they have mainly focused on the design and synthesis of functionalized isotropic nanostructures [3, 6, 11, 15-18]. Some other review articles, however, only discussed specific sensing mechanisms, such as growth and etching of plasmonic nanostructures [19-21], or specific applications, such as drug detection [22] and biosensing [23, 24]. Compared to their isotropic counterparts, anisotropic plasmonic nanostructures are considered more promising for colorimetric sensing because they offer a variety of advantages, such as widely tunable LSPR band and high optical sensitivity towards

changes in the local dielectric environment. These advantages facilitate the development of colorimetric sensors with better sensitivity, broader detection range, and higher visual resolution. However, to the best of our knowledge, only a few previous review articles have addressed this aspect in depth [25, 26]. Limited examples include the review article by Xia et al., in which three types of anisotropic nanostructures (nanorods, nanoplates, and nanoflowers) were discussed along with certain aspects of their colorimetric and fluorescent applications [25]. In another article by Yeung et al, the main focus was on the development of optical imaging techniques such as Dark-Field Microscopy, Differential Interference Contrast Microscopy, and Two-Photon Luminescence imaging Microscopy using anisotropic plasmonic nanostructures [26]. Nevertheless, synthesis of anisotropic plasmonic nanostructures has advanced significantly since then and more anisotropic nanocrystals with unique optical properties have recently emerged, which are promising for broader colorimetric applications with improved performances [27-31]. Furthermore, through surface modification and composite construction, anisotropic plasmonic nanostructures are now able to alter their optical properties in response to changes in temperature [32, 33], force [34], light [35], and magnetic field [36]. Some of these features have been exploited to design smart sensors, which appears to be an emerging topic [37]. It is reasonable to believe that an increasing number of colorimetric sensors based on anisotropic plasmonic nanostructures will be developed in the near future and applied to real-world domains.

Anisotropic plasmonic nanostructures

As shown in Table 1, Au nanomaterials with anisotropic structures, such as Au nanorods, nanoplates, nanoflowers, nanoframes, nanocubes, and nanobipyramids, have a higher sensitivity to changes in refractive index than low-dimensional spherical Au nanoparticles [38]. As their lengths grow and their vertices sharpen, the index sensitivity usually increases [39-41], presenting new opportunities for improving the sensitivity of colorimetric methods. In this section, we focus on the optical characteristics of these typical anisotropic nanostructures to illustrate why they are

suitable for colorimetric sensing applications. All of the anisotropic plasmonic nanostructures are discussed using Au as examples.

Table 1. Sizes, plasmon wavelengths, and refractive index sensitivities of diverse Au nanostructures [39-41]

Au	Length (nm)	Diameter/ thickness (nm)	Aspect ratio ^c	Plasmon wavelength (nm)	Index sensitivity (nm/RIU)	Figure of merit
Nanosphere	-	15	-	527	44	0.6
Nanoflower	80	-	-	1141	703	0.8
Nanocube	44	-	-	538	83	1.5
Nanoplate -	11	5	2.2	504	188	1.8
	197	14	14	1093	1096	4.3
Nanorod -	40	17	2.4	653	195	2.6
	74	17	4.6	846	288	1.7
Nanobipyramid—	50	18	2.7	735	212	2.8
	189	40	4.7	1096	540	4.5

Au nanorods

Au nanorods possess unique optical properties, which depend on their size and length-to-width aspect ratio [42, 43]. Unlike Au nanospheres, which have only one absorption peak, Au nanorods exhibit two LSPR peaks due to different polarization stemming from transverse surface plasmon resonance (~520 nm) and longitudinal surface plasmon resonance [44, 45]. The longitudinal surface plasmon resonance is extremely sensitive to the aspect ratio [46]. For example, when the aspect ratio increases from 1.7 to 5.2, the longitudinal plasmonic peak can move from 590 (visible range) to 935 nm (near-infrared (NIR) region). This change is accompanied by rich color changes in the Au nanorods solution [47]. Among all the anisotropic plasmonic

nanostructures, Au nanorods are the most common building blocks that have been used to design colorimetric sensors with an improved resolution to naked eyes.

Au nanoplates

Au nanoplates are a class of nanomaterials whose lateral dimensions are significantly larger than their thickness. Due to their special structure, the plate-like nanostructures exhibit a sensitive optical response to changes in their morphology and local dielectric environment [48]. Theoretical and experimental studies have revealed that faceted triangular nanoplates with sharp vertices provide enhanced electromagnetic field effects [49, 50]. Meanwhile, by adjusting the thickness and lateral dimension, their characteristic absorption peaks can shift approximately 600 to 1100 nm [41], making them good candidates for colorimetric sensing. Although Au nanoplates have high chemical stability, their synthesis by wet chemistry is always time-consuming and the yield is not ideal so that a centrifugation procedure is necessary to purify the nanoplates [51-53]. The plasmon-mediated synthesis approach can address this issue with considerably high yield [54, 55]. In general, the application of Au nanoplates in colorimetric sensing was rarely reported. In contrast, Ag nanoplates have found more applications in colorimetric sensing due to their ease of production, high yield, and high extinction coefficients, but their application has been limited by unsatisfactory stability and reproducibility. This disadvantage can be greatly alleviated by depositing a very thin layer of Au shell onto Ag nanoplates to form Ag@Au core-shell structures [56, 57].

Au nanobipyramids

Similar to Au nanorods, Au nanobipyramids are another type of elongated plasmonic nanoparticles with their longitudinal plasmonic band synthetically tunable from the visible region to the near-infrared region [58-60]. For Au nanorods, the rounded or flat end shapes provide a relatively small local electric field enhancement, thus limiting their applications for plasmonic enhanced spectroscopy. In addition, relatively wide size and shape distribution of Au nanorods may cause uneven widening of the longitudinal plasmonic peak [61]. In contrast, Au nanobipyramids possess two sharp tips, endowing them with larger local electric field enhancements, narrower peak

widths, and higher refractive index sensitivity [58]. Moreover, the approaches to the synthesis of Au nanobipyramids with uniform size and morphology homogeneity are robust and reliable. These features make Au nanobipyramids more promising candidates over Au nanorods for colorimetric applications.

Au nanoflowers

Au nanoflowers, also termed as Au nanostars or nanodendrites, are a collection of special three-dimensional nanostructures. These structures contain multiple sharp branches that greatly enhance the local electromagnetic field [62, 63], endowing them with higher catalytic activity than conventional Au nanoparticles with smooth surfaces. In addition, they have high exponential sensitivity and quality factors [40], so they have shown potential applications for surface-enhanced Raman scattering (SERS) [64], photodynamic therapy [65], and biosensing [66]. Their advantage in colorimetric sensing is that they have higher refractive index sensitivity than Au nanorods and Au nanobipyramids[40]. However, their spectral adjustability is less controllable than the above two because of the asymmetry and shape irregularity.

Au nanoframes

Au nanoframes are nanostructures with a hollow interior and a solid/porous wall thus possess high surface-to-volume ratio and low density. In addition, they have very strong plasmonic fields because of the coupling between their interior and exterior surface fields, greatly enhancing their index sensitivity [67]. They also have tunable LSPR characteristics which are highly dependent on their aspect ratio (wall length/wall thickness) [68, 69]. Synthesis protocols of hollow nanospheres, nanoplates, and nanocubes have been reported [70]. As they have a very high sensitivity factor (up to 408.8 nm/RIU) [71], Au nanoframes have great potential in the field of colorimetric sensing.

Au nanocubes

Compared with Au nanospheres, Au nanocubes are polyhedral nanoparticles with fewer faces and more vertices that show stronger surface plasmon resonance effects in a wider energy range [72, 73]. In addition, they exhibit a high photoluminescence quantum yield, which is 200 times higher than that of Au nanorods [74]. The electric fields are strongly confined in the vertices and edges of the nanocubes, making them advantageous plasmonic nanoantennae over nanospheres with similar size [75-77]. These enhanced local fields have been fully exploited for SERS and two-photon photoluminescence enhancement. Despite their striking plasmonic properties, however, attempts to use nanocubes in colorimetric sensing are rare probably due to the difficulty in modifying the nanocube surfaces. Nanocubes are usually capped with a cetyltrimethylammonium bilayer, which is difficult to replace [77].

Detection mechanisms

The optical properties of plasmonic nanostructures can be altered upon changing their interparticle distance, morphology, size, and composition. As shown in Fig. 1, the analyte-induced changes of these parameters are the underlying mechanisms for most plasmonic nanostructures-based colorimetric sensors. As one of the most distinctive features of anisotropic plasmonic nanostructures, their orientation-dependent optical properties have also been used to design novel sensors responsive to external stimuli, which are widely known as smart materials. Since these types of stimuli are usually physical, we discuss the development of smart materials in the next section. In this section, however, we focus on how the anisotropic plasmonic nanostructures were used to design colorimetric sensors for the detection of chemical and biological analytes. Overall, the mechanisms for colorimetric detection using plasmonic nanostructures usually fall into the manipulation of (1) interparticle distance, (2) morphology and size, (3) composition, and (4) alignment of nanostructures. As a result, the detection strategies can be classified into the following six types, analyte-induced aggregation, assembly, etching, growth, transformation, and orientation.

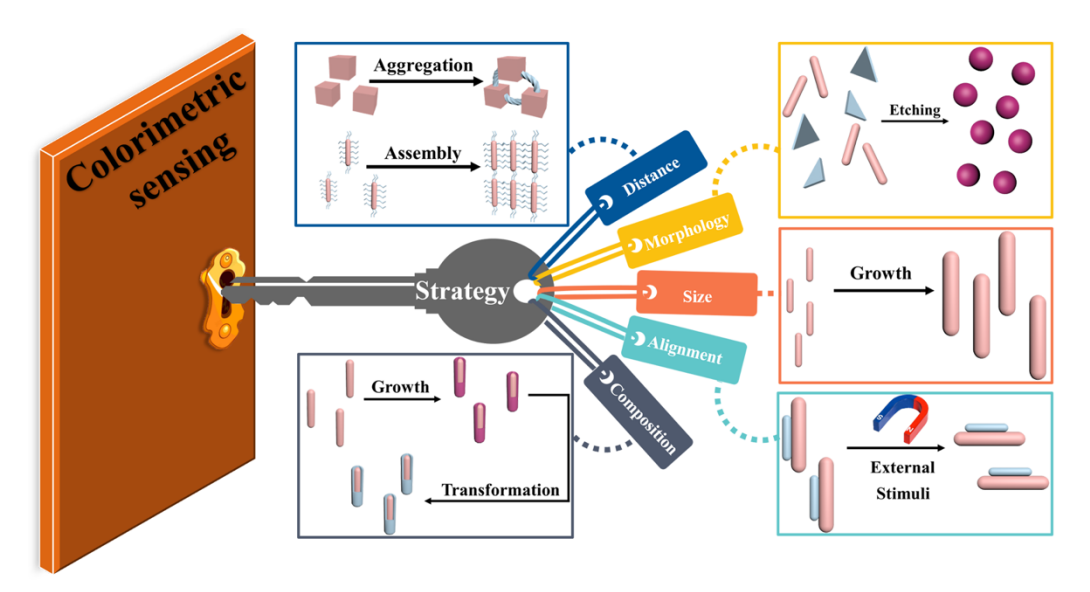


Figure 1. Scheme of anisotropic plasmonic nanostructures-based strategies for colorimetric sensing.

Change of interparticle distance Aggregation (Random assembly)

One of the most common strategies among these is the analyte-induced

aggregation that changes the interparticle distance of plasmonic nanostructures. In this case, the electromagnetic fields of nearby plasmonic nanoparticles are coupled due to the inter-particle proximity, leading to redshifts of plasmonic bands as a function of the analyte concentration. These redshifts of LSPR are accompanied by corresponding color changes, *e.g.* from red to blue for Au nanospheres, which can be used for visual detection. This strategy often follows the manners including hydrogen bond [78], electrostatic attraction [79], metal-ligand coordination [80], chiral interaction [81], immunological ligand-receptor binding [82], DNA hybridization [83], etc. For the above purposes, plasmonic nanomaterials generally require modifications with suitable functional ligands, which are able to complex with analytes and thus initiate their assembly. There have been many review papers summarizing the mechanism and development of this strategy using isotropic plasmonic nanostructures as signal transducers [3, 16, 18, 84], but we will focus on those referring to anisotropic plasmonic nanostructures.

Au nanorods are the most commonly used building blocks in these works. Typically, Au nanorods are synthesized through a seed-mediated growth method, in which cetyltrimethylammonium bromide (CTAB) is used as a surfactant for shapedirection and prevention of Au nanorods' aggregation. Teo et al. reported that CTABstabilized Au nanorods can be used for the colorimetric detection of dopamine by hydrogen bonding-driven aggregation [78]. In the presence of dopamine molecules, the ammonium bromide group on CTAB-modified Au nanorods can adsorb dopamine via electrostatic interaction. The hydrogen bonding among dopamine molecules decreases the interparticle distance of Au nanorods, inducing a color change from purple to colorless. Bamrungsap et al. [79] developed a colorimetric sensing system based on Au nanorods and graphene oxide for heparin detection using polydiallyldimethylammonium chloride as a molecular probe. The strong interaction between polydiallyldimethylammonium chloride and graphene oxide prevents the adsorption of Au nanorods on graphene oxide. In the presence of heparin, however,

polydiallyldimethylammonium chloride binds to heparin, inducing the aggregation of Au nanorods on graphene oxide via electrostatic attraction.

Metal-ligand coordination is another common strategy to induce the aggregation of plasmonic nanoparticles. Functional molecules containing amino, sulfur, hydroxyl, and/or carboxyl groups are widely used for this purpose because they can be easily bonded to the surface of plasmonic nanoparticles [80, 85-87], leading to their complexation with targeted metal ions and eventually to their aggregation. For example, Priyadars *et al.* [80] used meso-2,3-dimercaptosuccinic acid-modified Au nanorods to detect As⁵⁺ and As³⁺ ions, as these ions can bind with multiple thiol groups to form stable complexes, leading to the cross-linkage of Au nanorods (Fig. 2a). Colorimetric detection of metal ions using this metal-ligand coordination-induced aggregation strategy is summarized in Table 1. Similarly, glutathione, combination of glutathione and l-cysteine, lysine, 1-amino-2-naphthol-4-sulfonate, and plant extract have also been used to modify Ag nanorods, Ag nanoplates, Au nanoflowers and Ag@Au nanoframes for the detection of various metal ions including Co²⁺[88, 89], Ni²⁺[90], Hg²⁺[91], Fe³⁺ and As³⁺ [92] and Cd²⁺[93].

Discrimination of chiral compounds can be achieved by the design of aggregation-based colorimetric systems. In most chiral sensing systems based on spherical nanoparticles, chiral ligands or stabilizer molecules are modified on the plasmonic nanostructures to function as recognition units [94-97]. In addition, the intrinsic chiral recognition abilities of different types of plasmonic nanostructures were also exploited for the discrimination of chiral compounds. [81, 98-102] Li *et al.* used Au nanocubes to construct a chirally sensitive strategy for distinguishing leucine (Leu) enantiomers [81]. As shown in Fig. 2b, L-Leu can induce rapid aggregation of Au nanocubes, leading to the color change of Au nanocubes solution from red to colorless, which allows the visual detection of chiral isomers of Leu. On the contrary, D-Leu cannot induce the aggregation of Au nanocubes. Li *et al.* also synthesized CTAB-capped Au nanorods, which exhibited chiral selectivity towards D-glutamine over L-glutamine

[98]. To prove the intrinsic chirality of Au nanorods, they replaced CTAB with another ligand, i.e. thioglycolic acid, which played an insignificant role in chiral discrimination.

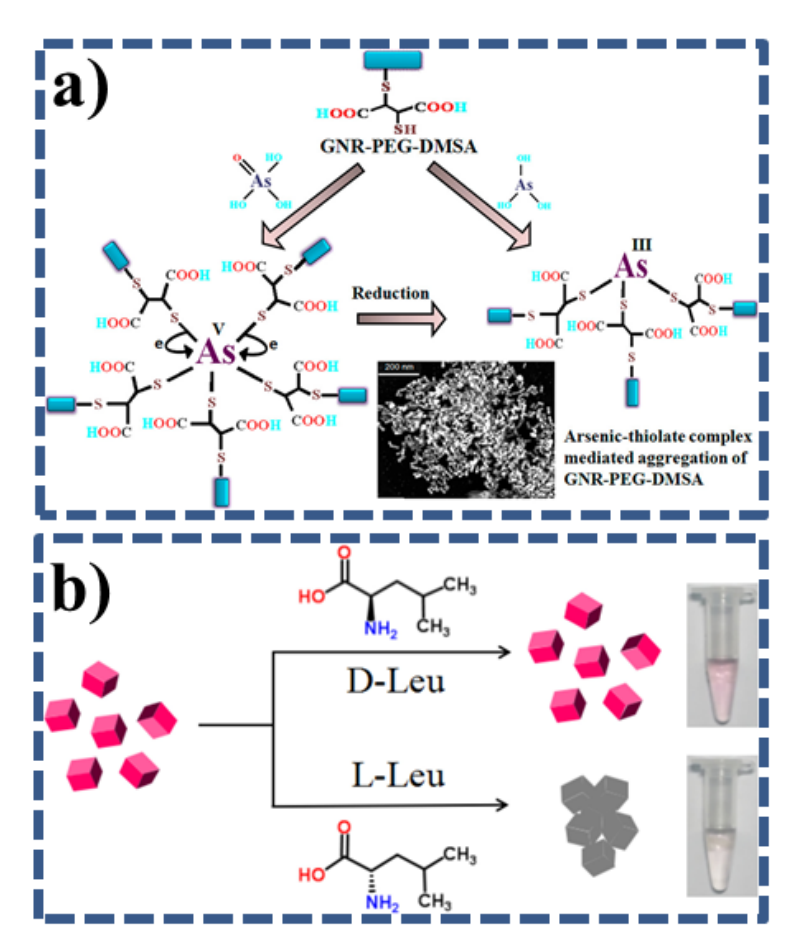


Figure 2. a) the interaction between Au nanorods-PEG-DMSA and As³⁺/As⁵⁺. Inset shows the SEM of aggregated Au nanorods after interaction with As³⁺/As⁵⁺. Reprinted from ref.[80] with permission; b) chiral recognition of L-Leu using cube-shaped Au nanoparticles as colorimetric probes. Reprinted from ref. [81] with permission.

Amongst all plasmonic nanostructures, Au nanoflowers possess most hierarchical structures with a rough surface and large surface-to-volume ratio, which benefits the adsorption and functionalization with antibodies and aptamers [82, 83]. Taking advantage of the specific recognition effect of antibodies and aptamers, these plasmonic sensors show high selectivity towards target analytes, making them promising for the direct analysis of biological samples with a complex matrix. In addition, the multiple sharp branches endow them with enhanced local electromagnetic field and improved optical signal response [103, 104]. These features make Au nanoflowers promising probes for colorimetric biosensing. Zhang *et al.* designed a hierarchical flowerlike

AuNPs probe for lateral-flow test strip immunoassay to detect *Escherichia coli* [82]. As shown in Fig. 3a, after antibody surface functionalization, Au nanoflowers agglomerate in the presence of the antigen (*Escherichia coli*). A remarkable improvement of detection sensitivity of tipped flowerlike AuNPs probes can be achieved as low as 10³ colony forming units (CFU)/mL by taking the above-mentioned advantages. In addition to antibodies, single-stranded DNAs were used for the conjugation with Au nanoflowers, which can be then used for the colorimetric detection of *Listeria monocytogenes* (Fig. 3b) [83]. To avoid complicated antibody modifications, Verma *et al.* directly used CTAB-capped Au nanoflowers as signal transducers by taking advantage of the electrostatic attraction between cationic Au nanoflowers and the intrinsic electronegativity of bacteria (Fig. 3c) [105, 106]. They were able to identify different strains of bacteria by using these Au nanoflowers with different sizes and branches aided with a linear discriminant analysis method.

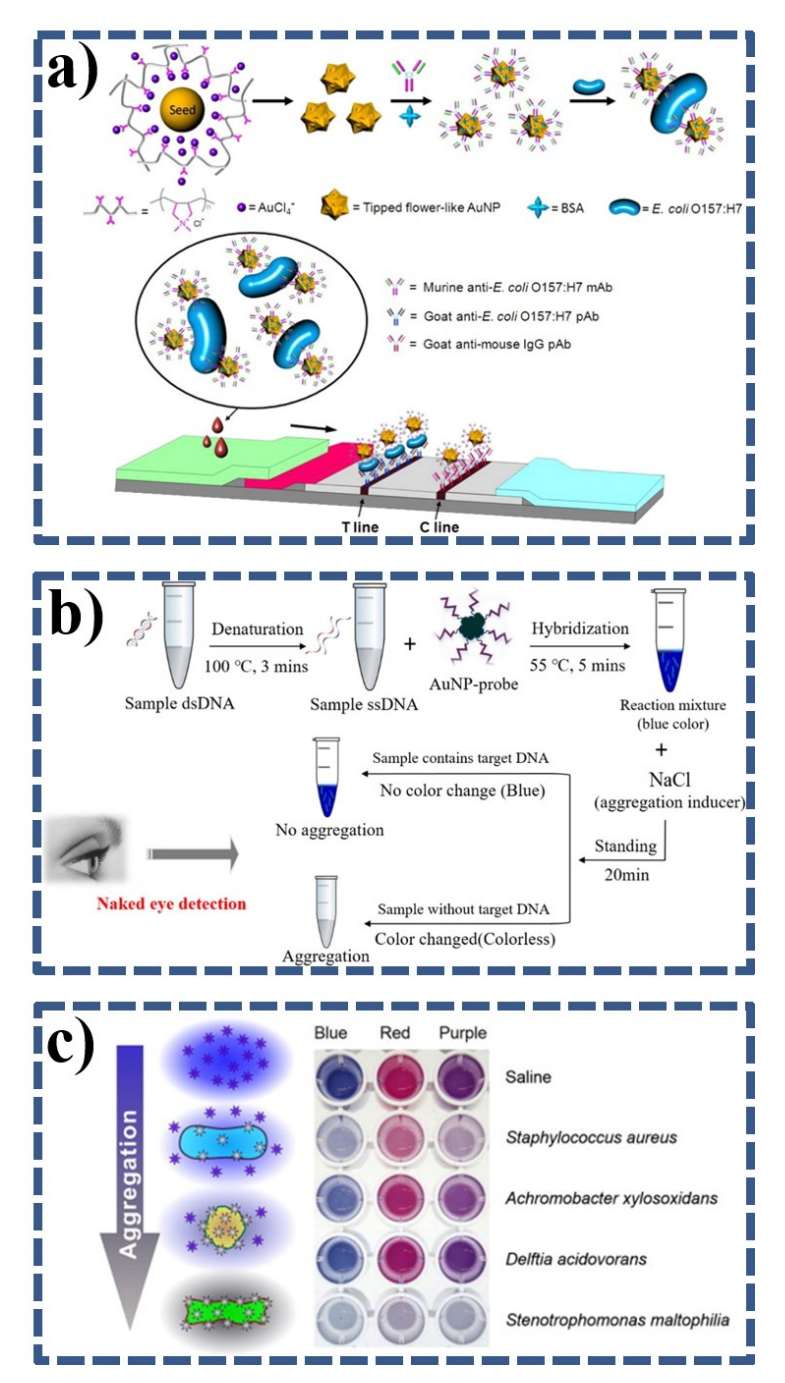


Figure 3. a) Schematic illustration of surface functionalization of Au nanoflowers with antibody I (Murine anti-E. coli O157:H7 mAb) and BSA, and LFTS detection of E. coli O157:H7. Reprinted from ref. [82] with permission; b) Scheme of a colorimetric assay for the detection of DNA using Au nanoflowers-based hybridization. Reprinted from ref. [83] with permission; c) Change in color of Au nanoflowers caused by varying degrees of aggregation due to the differences in surface charge, surface area and morphology of bacteria. The photograph shows the color when species of bacteria with final OD_{660} =0.02 are added to different Au nanoflowers. Reprinted from ref. [106] with permission.

Another strategy to manipulate the interparticle distance is based on the antiaggregation of plasmonic nanoparticles in the presence of target analytes. This strategy

relies on those highly functionalized compounds, which have multi-amino and/or -thiol groups [107-110]. Due to their strong complexing and crosslinking ability, the addition of these highly functionalized compounds into the nanoparticles matrix can result in their aggregation, which can be either prevented or interfered by the analytes of interest because the analytes have a stronger binding affinity towards the functionalized compounds than that of plasmonic nanoparticles. Therefore, the color variation from red to blue (e.g., for Au nanoparticles) is inhibited as a function of the analyte concentration. Taking advantage of these properties, an anti-aggregation method was developed for the colorimetric detection of Hg²⁺ using dithiothreitol (DTT) and Au nanorods [107]. DTT, which has two thiol groups, can lead to the assembly of Au nanorods. This assembly will be inhibited by the existence of Hg²⁺ as it has a higher binding affinity towards DDT than Au nanorods do. Bi et al. have also developed a colorimetric method for the detection of Hg²⁺ ions using Au nanorods based on the above principles [111]. In their method, 6-mercaptopurine was used to induce the aggregation of Au nanorods by forming the Au-S bond. In the presence of Hg²⁺, the aggregation is suppressed due to the formation of a more stable Hg-S bond. Xu et al. developed a colorimetric method for detecting DNA molecules based on the antiaggregation of Au nanorods with the amplification strategy of hybridization chain reaction [112]. Without target DNA, Au nanorods undergo aggregation due to the weak protection of hairpin DNA, while in the presence of target DNA, the hybridization of hairpin DNA is initiated to form a double-helix structure, which adsorbs tightly with Au nanorods due to strong electrostatic attraction. This prevents Au nanorods from aggregating under high ionic strength.

It should be noted that fewer efforts have been made to design aggregation or antiaggregation based colorimetric sensors using anisotropic plasmonic nanostructures than that using isotropic ones. This might be due to the fact that the color variation gradients of sensors using anisotropic plasmonic nanostructures as building blocks are not superior to those using isotropic ones, while their synthesis protocols are usually more complicated.

Oriented assembly (Side-by-side and End-to-end)

Different from those cases of random aggregation, there are two types of highly oriented assembly modes for Au nanorods, i.e., side-by-side and end-to-end [113, 114]. The well-controlled assembly is often achieved through the passivation of a specific facet of Au nanorods and subsequently initiates the assembly from the active facet. For Au nanorods synthesized by the typical seed-mediated growth method, a layer of CTAB preferentially binds to the (110) facet, which is the longitudinal side of Au nanorods, leaving more exposed facets at the tips for ligand modification. As a result, the end-toend assembly of Au nanorods is commonly used to design the colorimetric sensing. For example, as shown in Fig. 4a-c, Lu et al. reported the colorimetric detection of organophosphate pesticides (OPs) based on the enzymatic reaction-modulated end-toend assembly of Au nanorods [115]. Cysteine, a type of amino acids possessing both thiol and amino groups, can selectively bind to the tip of Au nanorods inducing end-toend assembly of Au nanorods. In the presence of cholinesterase (ChE), such assembly was disrupted as thiocholine generated by ChE catalysis can compete with cysteine to bind with the tip of Au nanorods. As ChE was incubated with OPs, the enzymatic activity was inhibited, and the assembly appeared again. Chen et al. proposed a Hg²⁺ detection system by taking advantage of the end-to-end self-assembly of Au nanorods [116]. They showed that Hg²⁺ ions can be reduced to Hg⁺ ions forming gold amalgams at the tip of Au nanorods. The produced Hg⁺ ions can then complex with lysine, leading to the end-to-end assembly. Accordingly, the longitudinal LSPR band of Au nanorods disappeared gradually with the emergence of a new band at 900-1100 nm. These spectral changes are dependent on the concentration of Hg⁺ ions. Similarly, Wang et al. developed a method for lysine detection based on the end-to-end self-assembly of 11mercaptoundecanoic acid-modified Au nanorods [117]. The coordination binding among Eu³⁺, lysine and 11-mercaptoundecanoic acid as well as the electrostatic interaction between lysine and 11-mercaptoundecanoic acid contributed to the end-toend assembly of Au nanorods.

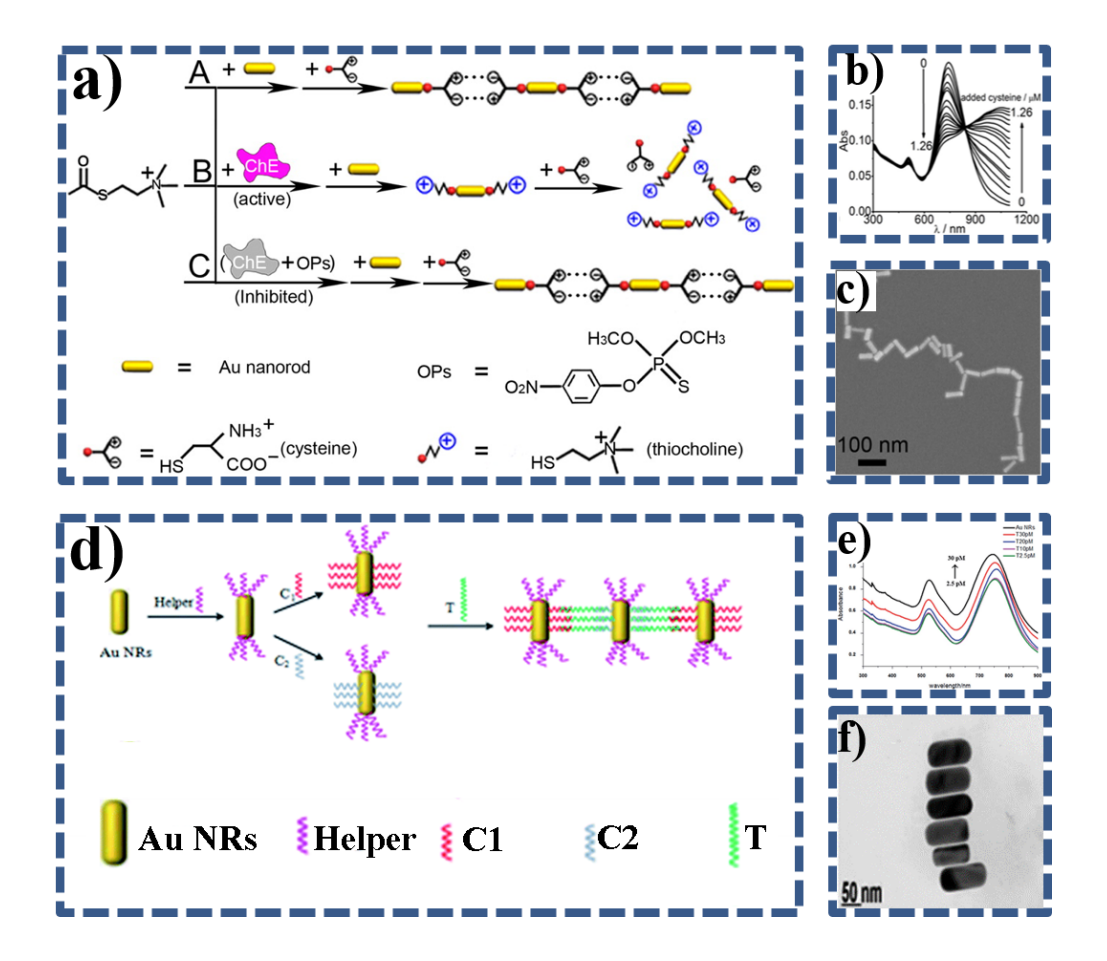


Figure 4. a) Schematic illustration of a colorimetric assay for ChE and OPs based on the modulation of end-to-end assembly of Au nanorods. A. In the absence of ChE, Au nanorods end-to-end assemble with each other induced by cysteine. B. In the presence of ChE, the enzymatic thiocholine prevents the cysteine-induced end-by-end self-assembly of Au nanorods. C. in the presence of OPs, the enzymatic activity is inhibited, and the cysteine-induced Au NR end-to-end assembly is observed again; b) UV-vis spectra of the Au nanorods upon addition of cysteine; c) SEM image of the Au nanorods upon addition of cysteine. Reprinted from ref.[115] with permission; d) Schematic illustration of side-by-side assembly designed for the detection of DNA; e) UV-vis spectra of the Au nanorods upon addition of target DNA; f) TEM images of Au nanorods assembled into side-by-side structures. Reprinted from ref.[118] with permission.

The side-by-side assembly has also been used to design colorimetric sensors. For example, a thiolated DNA sequence, which was not responsive towards target DNA, was used to passivate the tip of Au nanorods (Fig. 4d) [118]. Another two DNA sequences that are complementary to the target DNA, were functionalized on the side surface of Au nanorods, triggering side-by-side assembly in the presence of target DNA (Fig. 4f). Fig. 4e shows that the intensity of transverse peaks decreased with a minor blue shift from 525 nm to 521 nm, while the intensity of longitudinal peaks inclined

with a redshift from 742 to 751 nm. Another strategy enabling the side-by-side assembly was proposed based on the electrostatic attraction of ligand on the side face, which further crosslinks the Au nanorods side by side in the presence of analytes. For example, Zhang *et al.* reported a visualized detection of alpha-fetoprotein (AFP) using Au@Ag core-shell nanorods [119]. The Au@Ag nanorods modified by positively charged CTAB electrostatically adsorbed negatively charged AFP on their side face and then induced side-by-side aggregation. Compared to pristine Au nanorods, the introduction of the silver shell produces a more tunable LSPR property, thereby providing more significant color changes. Similarly, Guan *et al.* developed a visual detection method for Hg²⁺ based on the side-by-side assembly of L-arginine-functionalized Au nanorods [120]. The L-arginine can be deprotonated under suitable pH, and then adsorbed onto the side face of Au nanorods by the bilayer of positively charged CTAB layer. When Hg²⁺ ions exist, the deprotonated amine group of L-arginine on the Au nanorods binds with Hg²⁺ and leads to the assembly of Au nanorods, resulting in a color change from red to green.

Morphology, size, and composition change

The above-mentioned colorimetric methods based on the analyte-modulated changes of interparticle distance have gained tremendous attention over the past decades. However, they often require a time-consuming and complicated functionalization step, which limits their practical applications. In addition to the interparticle distance, the LSPR of plasmonic nanostructures is highly dependent on their size, morphology, composition, and orientation. As a result, colorimetric sensors can also be developed by designing systems based on the analyte-induced changes of those parameters. There are three methods to achieve this purpose. The first one is based on the analyte-inducing deposition of (new) metals onto the original plasmonic nanostructures. The second one is based on the analyte-initiating etching of plasmonic nanostructures. The last one is based on the analyte-triggering composition transformation of the plasmonic nanoparticles. In these methods, anisotropic plasmonic nanostructures not only provide a lower detection limit due to their higher

sensitivity to changes in the refractive index but also offer wider detection range and better visual resolution due to their more tunable optical properties.

Etching

It is well-known that noble metals, particularly gold, are stable because they are difficult to be oxidized. The standard electrode potential of Au^+/Au ($\phi^{\theta}(Au^+/Au)$) and Ag^+/Ag ($\phi^{\theta}(Ag^+/Ag)$) is 1.69 V and 0.80 V, respectively. To facilitate the etching of gold, anions such as cyanide (CN⁻), halides (X⁻), and thiosulfate (S₂O₃²⁻) are required to complex with gold to decrease its oxidative potential. For example, when Br and CN⁻ complex with gold, the value of $\varphi^{\theta}(Au^{+}/Au)$ decreases to 0.96 V and 0.57 V $(AuBr_2^-+e^-\rightarrow Au+2Br^-, \phi=0.96 \text{ V};$ $4Au+8CN-+2H_2O+O_2\rightarrow 4[Au(CN)_2]-+4OH^$ φ=0.57 V), thereby making the oxidative etching of gold more readily. Overall, etching-based methods can be mainly classified into four types: (1) direct etching of plasmonic nanostructures by analytes which have high oxidative potentials such as $H_2O_2[121, 122], Hg^{2+}[123-127], As^{5+}[128], Cr^{6+}[129], ClO^{-}[130-132] and NO_2^{-}[133];$ (2) indirect etching of plasmonic nanostructures by analytes (e.g., Hg^{2+[134]}, Pb²⁺[135], CN⁻[136-138], halogen ions [139, 140] and S₂O₃²⁻) via forming metal-analyte complex or alloy ([Au(CN⁻)₂]⁻ complex and Au-Hg alloy, etc.) which decrease the electrode potential of metals; (3) analyte-triggered (e.g. enzyme-linked immunosorbent assay (ELISA)) generation of strong oxidants such as H₂O₂ [141], I₂ [142-145], 3,3',5,5'tetramethylbenzidine (II) (TMB²⁺) [146-148], and superoxide radical (O₂·-) (or termed as hydroxyl radical (OH) [149-152]; (4) inhibitive etching of plasmonic nanostructures by the analytes due to their strong reactive affinity towards etchant. In these methods, Au nanorods, Ag nanoplates, and Au nanobipyramids are primarily used because the etching of these plasmonic nanostructures can induce a broad shift of LSPR band, which will bring sharp-contrast multicolor changes. In addition, unmodified plasmonic nanostructures can be used directly for the detection of target analytes, thereby eliminating any additional steps for surface functionalization.

The most straightforward approach is based on utilizing the strong oxidative capacities of analytes to etch gold or silver under certain conditions. For example,

CTAB-stabilized Au nanorods can be etched by Cr^{6+} as the value of $\phi^0(Cr^{6+}/Cr^{3+})$ (1.33 V) is higher than that of $\phi^0([AuBr_2]^7/Au)=0.96$ V. As a result, a colorimetric method was proposed to detect Cr^{6+} using CTAB stabilized Au nanorods [129]. Upon exposure to Cr^{6+} , Au nanorods were etched into spherical shapes, along with a color change from wine red to yellow, and eventually to colorless. Similarly, a colorimetric sensor for benzoyl peroxide (BPO) and H_2O_2 detection was developed by etching Au@Ag nanorods [121, 122] . As shown in Fig. 5a, BPO, and H_2O_2 can oxidize Ag nanoshells of Au@Ag nanorods; the etching of Ag nanoshells changes the aspect ratio of Au@Ag nanorods, resulting in corresponding spectral and color changes (Fig. 5b-c). Ag nanoplates can also serve as signal transducers for the detection of H_2O_2 [153, 154]. In the presence of H_2O_2 , the Ag nanoplates are eroded, and their morphology changes from triangles to circles, resulting in the disappearance of LSPR band at 400 nm and a significant decrease in the absorption intensity at 670 nm. The color change of the reaction system from the initial blue to lavender can be observed.

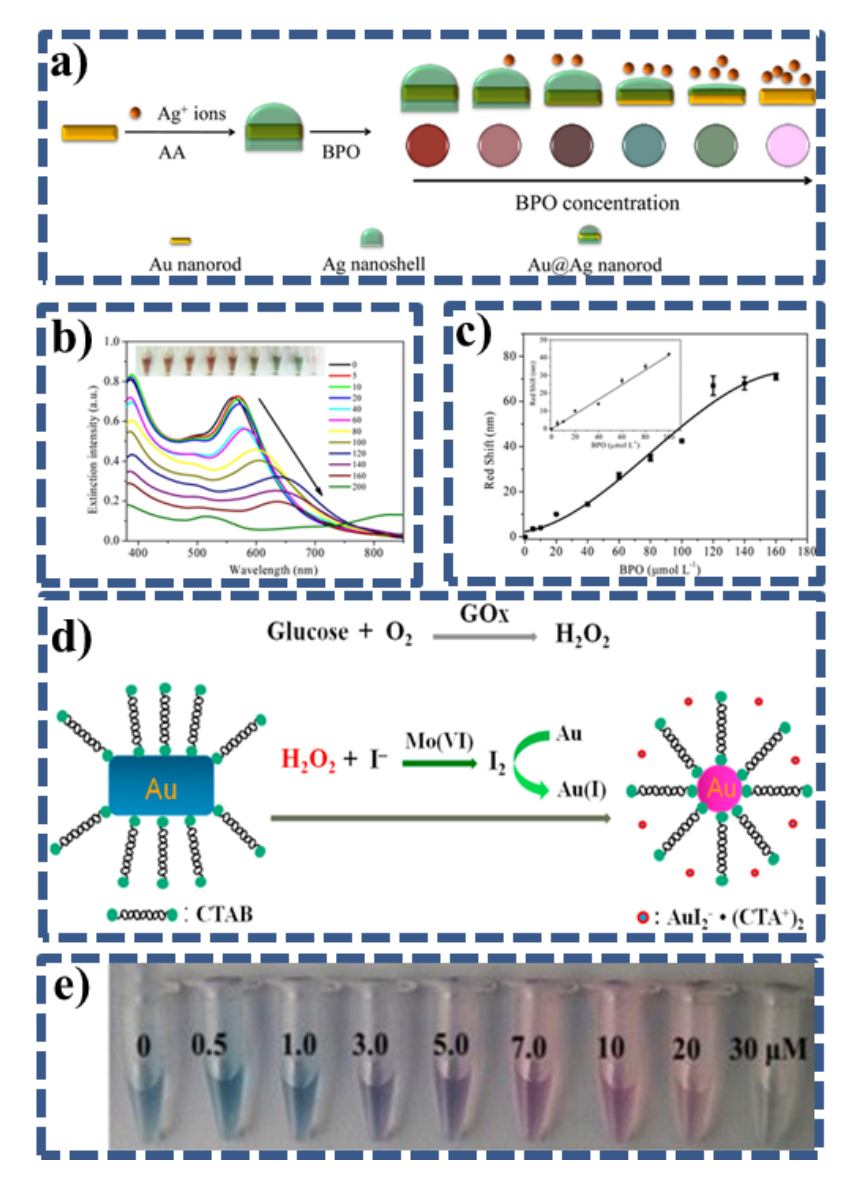


Figure 5. a) Schematic illustration of colorimetric detection of BPO using Au@Ag nanorods as the signal transducer; b) UV-vis spectra of Au@Ag nanorods colloidal solution in the presence of different concentrations of BPO. Inset is the corresponding photos of colloidal solutions in the presence of different concentrations of BPO (from left to right: 0, 5, 10, 20, 40, 60, 80, 100, 200 mol L⁻¹); c) Red-shift of longitudinal LSPR peak of the colloidal solution as a function of BPO concentration. Reprinted from ref.[121] with permission; d) Schematic illustration of the Au nanorods-etching-based glucose sensor; e) Photographic image of Au nanorods colloidal solution after incubation with different concentrations of glucose in acetate buffer at 45 °C for 25 min. Reprinted from ref.[141] with permission

Anions or cations that can form metal-analyte complexes or alloys are also used to decrease the electrode potential of gold or silver, making them easier to be oxidized. Cyanide is known to be highly nucleophilic and can form a very stable complex with metals such as gold and silver. The stability constant of $[AuCN_2]^-$ and $[AgCN_2]^-$ complex is as high as 2.0×10^{38} and 1.3×10^{21} , respectively. As a result, the standard

potentials of gold and silver decreased to 0.57 and -0.45 V upon complexing with cyanide, making them readily oxidizable by oxygen. Benefitting from this property, a series of colorimetric methods were developed for the detection of cyanide using Au or Ag nanostructures [136-138]. For instance, cyanide can etch Au nanorods preferentially along the longitudinal direction due to less surface passivation and higher reaction activities at the tips of Au nanorods, resulting in a decrease of Au nanorods' aspect ratio and a blue-shift of LSPR absorption (i.e., color changes from peacock blue to pink) [138]. Halide and thiosulfate ions play similar roles as cyanide [135, 155, 156]. In addition to anions, cations (e.g. Pb²⁺ions) that can form alloys with gold and silver can decrease their electrode potentials. A colorimetric method for the detection of Pb2+ was established by taking advantage of the Pb²⁺-accelerated etching of Au nanorods [135]. In this method, Pb²⁺ ions can form a monolayer of AuPb₂ and AuPb₃ alloys on the gold surface to decrease its electrode potential, thus accelerating the dissolution of Au nanorods in the presence of S₂O₃²⁻ and changing its shape into nanospheres. This morphological transformation leads to a blue shift and damping of the longitudinal LSPR absorption band of Au nanorods, which eventually merges into the transversal absorption.

Some target molecules can react with specific parent compounds to produce reactive intermediates with high oxidative ability. This mechanism has also been used to design colorimetric sensors. For example, Fe²⁺ and Co²⁺ can initiate the Fenton reaction to produce O₂⁻⁻, which can etch Au nanorods [157, 158]. Similarly, a method was developed for the colorimetric detection of urine glucose [141]. Catalyzed by MoO₄²⁻, Au nanorods were efficiently etched by H₂O₂ which was generated by glucose-glucose oxidase (GOx) enzymatic reaction (Fig. 5d), accompanied by a color change from blue to red, and colorless (Fig. 5e). For enzyme-linked immunosorbent assay (ELISA)-mediated etching, the underlying mechanism is based on enzymes that can catalyze target molecules to produce etchants such as H₂O₂[141, 159]. ELISA is known for its high selectivity due to the specific recognition between antibody and antigen. Therefore, sensors developed based on this strategy exhibit high specificity towards

analytes. For instance, Xiong et al. developed a method for the colorimetric detection of aflatoxin B1 (AFB1) in corn samples based on ELISA-assisted etching of Au nanorods [149]. As shown in Fig. 6a, the AFB1@GOx conjugates can be captured by anti-AFB1 mAbs on the plate well. Then, the glucose was oxidized by GOx to generate the H₂O₂, which can etch the Au nanorods into Au nanospheres producing color changes from bluish-green to light red. However, in the presence of AFB1, the anti-AFB1 mAbs preferentially bind with the AFB1 molecules, and thus only bluish-green color was observed because the Au nanorods retained their rod-like morphology. A similar mechanism has also been used for the colorimetric detection of telomere activity [150] and microRNA 141 (Fig. 6b) [151] based on the horseradish peroxidasemimicking DNAzyme-assisted etching of Au@Ag nanorods. Compared to Au nanorods, Au nanobipyramids have proven to be a better candidate probe for this ELISA-based etching strategy because it can improve the sensitivity by orders of magnitude due to its sharp-tip enhanced optical sensitivity[160] and vivid color responses. This is because Au nanobipyramids have much larger extinction crosssection and local electric field enhancement than Au nanorods, resulting in higher sensitivity to the changes of the refractive index. For example, the colorimetric detection of squamous cell carcinoma antigen was achieved by catalase-guided etching of AuNBPs@Ag [161]. As shown in Fig. 6c, the original AuNBPs@Ag is standard stick shape with a solution color of brownish-yellow. After part of the silver is etched, the stick-like nanostructures transform into a rice-like shape while the solution color turns to green. After all silver is etched, the shape turns to Au nanobipyramids and the solution color becomes reddish-brown. Further etching of Au nanobipyramids results in "walnut-like" and quasi-spherical shapes, leading to the color change from reddishbrown to blue and then pink. Thus, the target concentration can be easily identified with visual detection, with a limit of detection of 2.5 ng/mL.

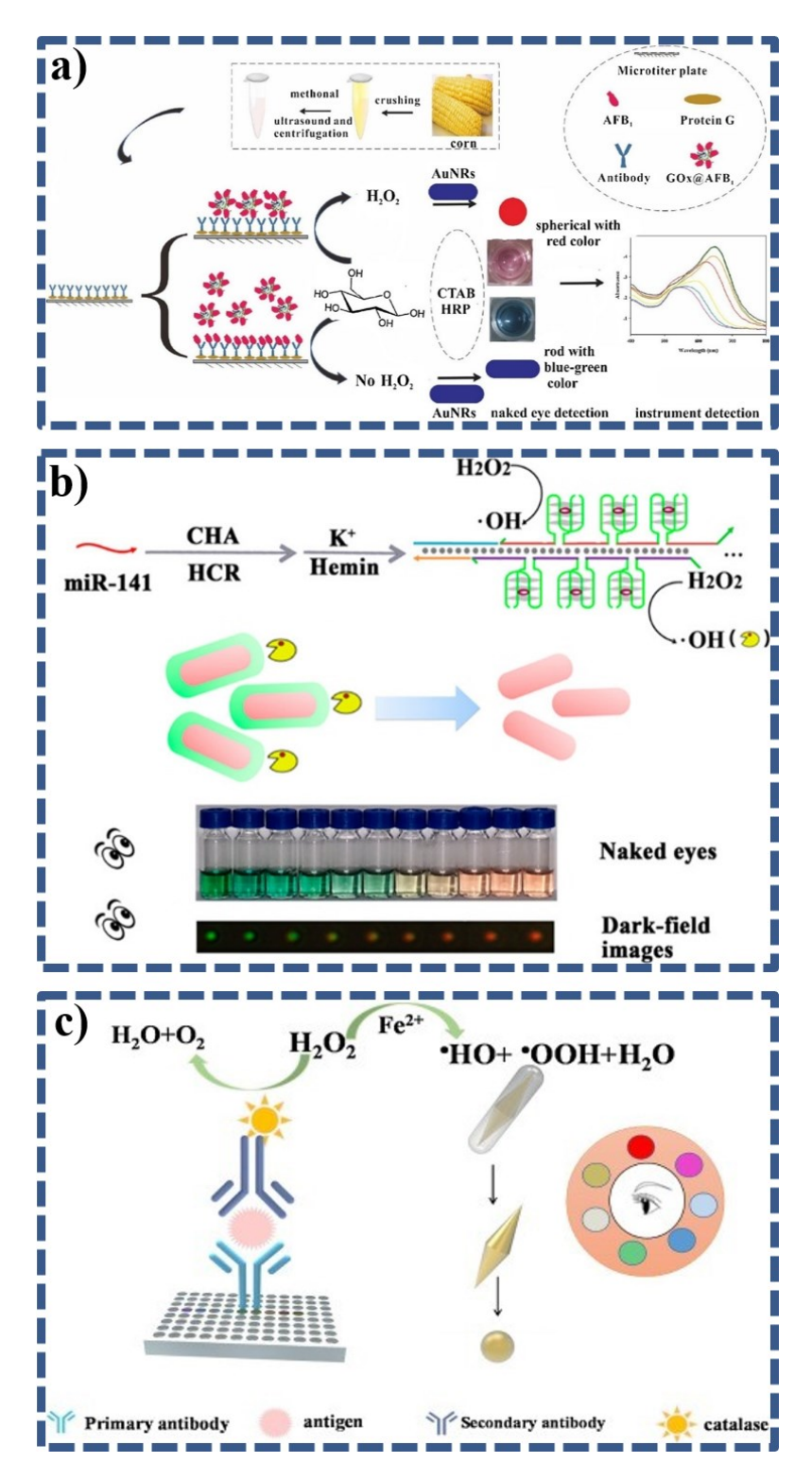


Figure 6. a) Scheme of the proposed AuNR-etching-based competitive pELISA for the naked-eye detection of AFB₁. Reprinted from ref. [149] with permission; b) Schematic illustration of the principle for determination of miR-141. Reprinted from ref. [151] with permission; c) Schematic illustration of the proposed immunosensor for the colorimetric detection of squamous cell carcinoma. Reprinted from ref. [161] with permission.

An inhibitive-etching approach was proposed as the analytes prefer to react with

etching agents, thus protecting the plasmonic nanostructures from being etched. For example, Yuan *et al.* developed a method to detect biothiols based on the inhibitive-etching of Au nanorods by the Fenton reaction [162]. The etching of Au nanorods is inhibited to a varying extent when adding different concentrations of biothiols, which can bind to the (111) facet of Au nanorods through Au-S bonding thus preventing the etching. Based on a similar principle, superoxide dismutase activity [163], cysteine [164], H₂S [165], ascorbic acid [166], glutathione and thiocholine [167], OPs [168, 169], nicotinamide adenine dinucleotide [170], Cu²⁺ [171], and herbicide aminotriazole [172] can be detected. Ag nanoplates can be also used for signal output by this strategy. Fang *et al.*[173] proposed a colorimetric method to detect dopamine in serum. In the presence of dopamine, Ag nanoplates were protected from etching by Cl⁻. In the absence of dopamine, the Ag nanoplates were etched into round nanodisks. Other than dopamine, such an analyte-induced protective etching strategy using Ag nanoplates has also been reported for the detection of thiols [174], glucose [175], blood uric acid [176], providing new approaches for bio-sensing.

Deposition (growth)

Generally, deposition-based detection relies on the epaxial growth of new metals onto the original plasmonic nanostructures, which can be achieved by target-triggered reduction of metal precursors. It is common that the deposited metals have similar crystal lattice as the original plasmonic nanostructures. Since silver and copper are compatible with gold in terms of the crystal lattice, reduction of their salts is usually applied to this type of colorimetric sensors. For example, a colorimetric sensor array has been developed for the detection and discrimination of catecholamines based on their ability to reduce silver salts (Ag⁺) to deposit silver on the surface of Au nanorods [177]. Formaldehyde (HCHO) can also reduce Ag⁺ to Ag on the surface of Au nanorods to form Au@Ag core-shell nanorods. Based on this fact, Lin *et al.* and Duan *et al.* developed colorimetric sensors for the determination of HCHO using Au nanorods coupled with Ag⁺-glycine-sodium hydroxide [178] and Tollens reagent [179] (Fig. 7a-f). Lin *et al.* developed a colorimetric method for the detection of p-aminophenol in

environmental water and human urine samples based on the preferential deposition of Ag on the concave Au nanorods [180]. They also explored a strategy for visual detection of biogenic amines with multiple color changes based on hydrolysis-induced silver metallization reaction to tune the LSPR adsorption of Au nanorods [181]. It is also viable to develop strategies based on analyte-induced gold deposition onto Au nanorods to change their original morphology and size. For example, Kashani et al. presented a method for colorimetric detection of glutathione (GSH) using Au nanorods (Fig. 7g). The mechanism of the sensor is based on shifting the LSPR during selective transverse overgrowth of gold induced by preferential binding of GSH at the nanorods' tips [182]. However, the LSPR peak shift resulted from the deposition of gold onto Au nanorods was insignificant, thus only resulting in the color change from dark to light purple (Fig. 7h). In addition to the deposition of metals, polymeric complexes such as dithiothreitol-Pb²⁺[183] (Fig. 7i-j) and rhodanine-Hg²⁺[184] can be formed around Au nanorods and Au nanobipyramids, changing the dielectric environment near the nanoparticle surface. Thus, colorimetric sensing of Pb²⁺ and Hg²⁺ can be achieved by recording the spectral and color changes.

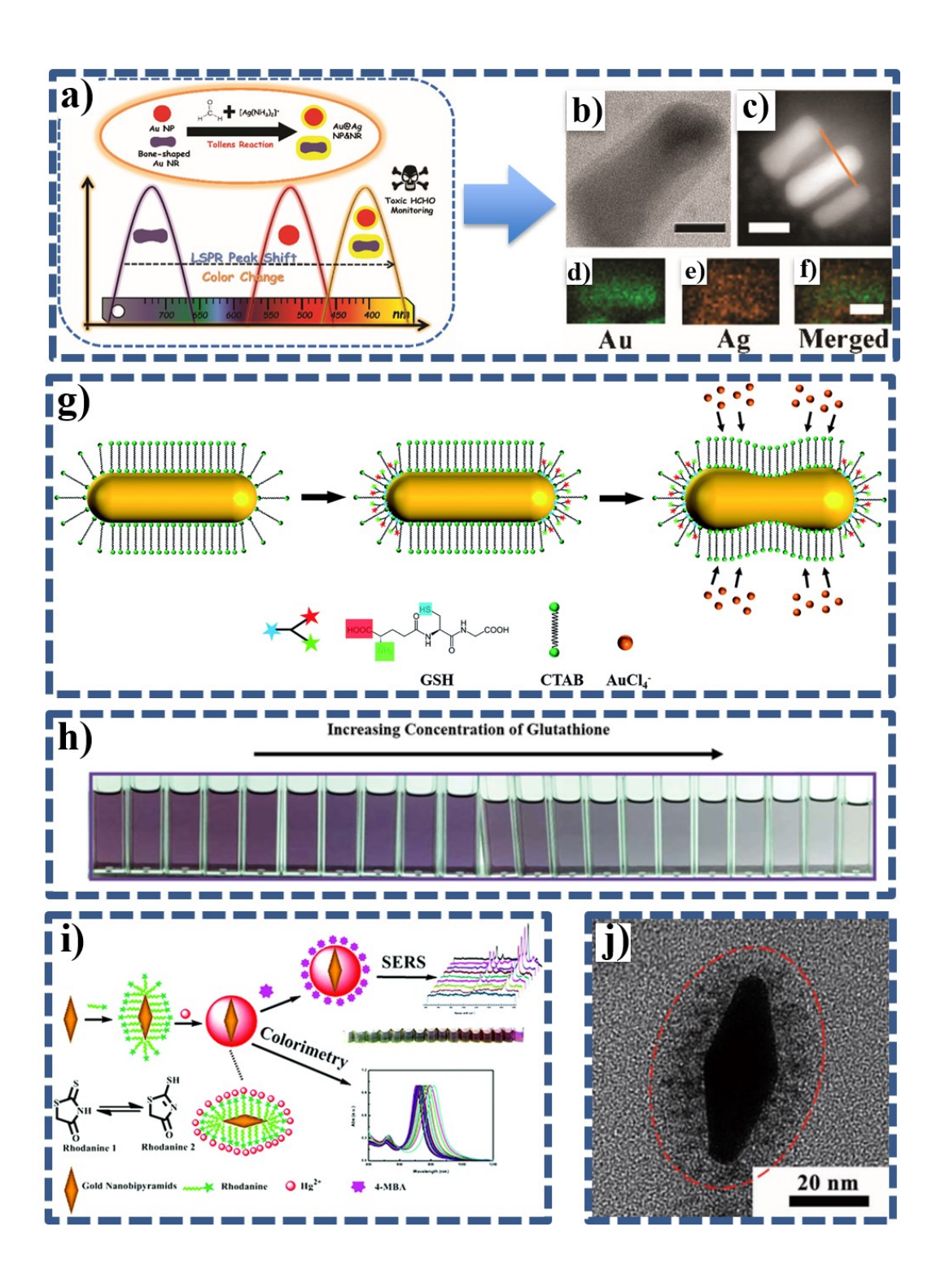


Figure 7. a) Schematic illustration of the plasmonic detection of HCHO based on Au nanoparticles or Au nanorods coupled with classical Tollens reaction; b) an HRTEM image, c) corresponding HAADF-STEM image and d)-f) EDX elemental maps of the products of the reaction between bone-shaped Au nanorods-Tollens reagent and HCHO (all scale bars are 20 nm). Reprinted from ref.[179] with permission; g) Graphical illustration for transverse overgrowth on Au nanorods induced by GSH; h) Colorimetric determination of GSH based on transverse overgrowth of nanorods induced by varying concentration of GSH at optimum condition. Reprinted from ref.[182] with permission; i) Schematic illustration of the formation of a partition layer on the surface of the Au NBs and the dual-modal sensing of Hg²⁺; j)TEM image of the corresponding rhodanine-stabilized AuNBs reacting with 5.0×10^4 M Hg²⁺. Reprinted from ref.[184] with permission.

ELISA is another common method to induce the reduction of new metals onto original plasmonic nanostructures for sensing purposes. As illustrated in Fig. 8a-e, alkaline phosphatase (ALP) is introduced by immunoreaction with a target antigen (prostate-specific antigen in this case) [185]. The ALP can catalyze the dephosphorylating of p-aminophenol phosphate to produce p-aminophenol, which will further reduce silver ions into metallic silver, resulting in the deposition of silver onto Au nanorods. The corresponding spectral and color changes can be utilized for the detection of target antigens. Based on this principle, Li et al. developed a strategy for the colorimetric detection of prostate-specific antigens based on the ELISA-triggered growth of Au nanorods by ascorbic acid, which was induced by the dephosphorylating of ascorbic acid-phosphate with ALP [186]. By modifying different antibodies, this strategy can be adapted for the detection of other antigens such as the H₅N₁ virus [187] (Fig. 8f-1) and ochratoxin A[188] (Fig. 8m) using Au nanobipyramids and Au nanoflowers for signal readout. Zhang et al. [189] developed an enzyme-modulated colorimetric assay to measure lipase activity. The method relied on enzymatic reactionassisted gold deposition on Au nanorods to generate a color change from red to dark blue, which was strongly dependent on lipase activity. Chen et al. developed an enzyme-induced metallization colorimetric assay to measure beta-galactosidase (β-gal) activity, which was further employed for bacteriophage-enabled colorimetric detection of Escherichia coli [190]. In the presence of β-gal, the hydrolysis reaction produced paminophenol, which further reduced silver ions to form a silver shell on the surface of Au nanorods.

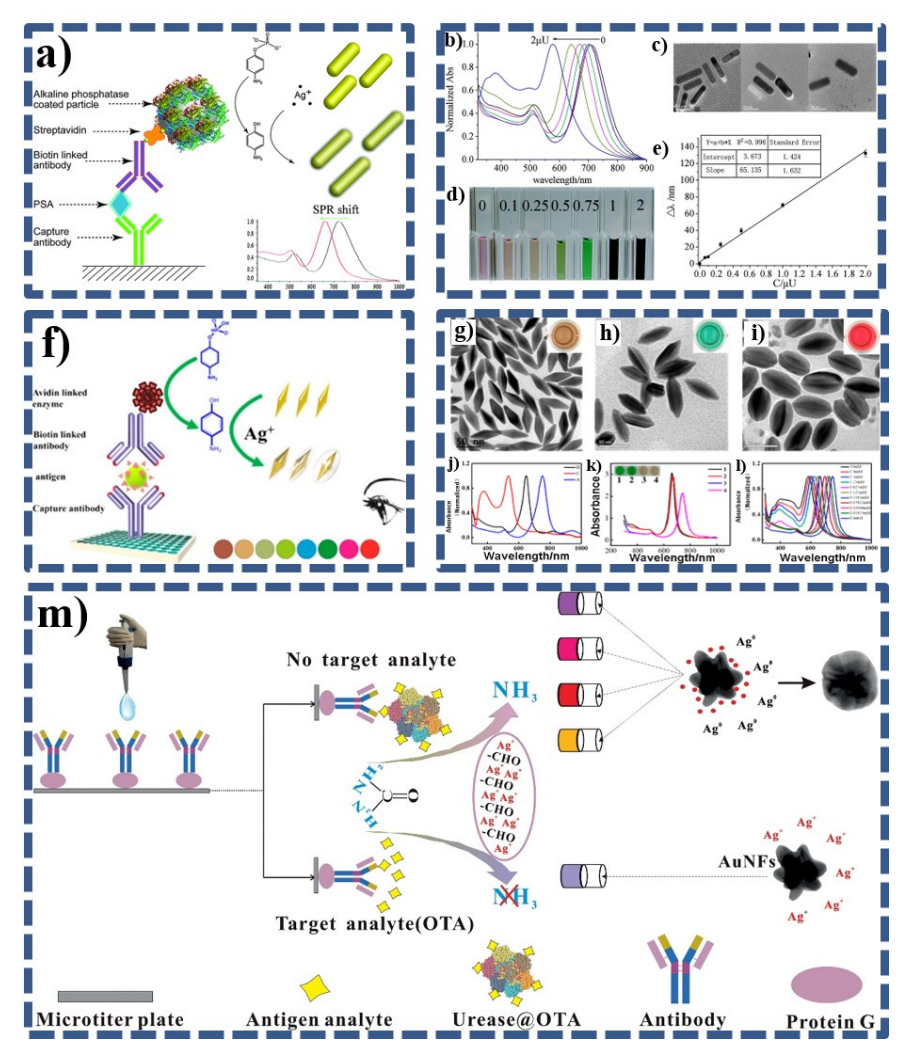


Figure 8. a) Schematic illustration of the working principle of the prostate-specific antigen assay b) UV-vis spectra of the Au nanorods at different concentrations of ALP. c) TEM images before and after the enzyme-catalyzed deposition of silver (1-3: 0, 0.5, 2 µU ALP) d) The color change of the Au nanorods at different concentrations of ALP. e) the correlation between the activity of ALP and the SPR shift of the Au nanorods derived from b). Reprinted with permission from ref. [185]; f) Schematic illustration of the principle of the proposed immunosensor (g-i) TEM and (j) UV-vis absorption spectra of the Au nanobipyramids with the deposition of a silver shell with increasing thicknesses induced by H5N1 at increasing concentrations. When H5N1 existed, the capture antibody (Ab1), antigen, and detection antibody (Ab2) formed a sandwiched immunocomplex (Ab1-antigen-Ab2) via antibody-antigen interaction. Then it was conjugated with alkaline phosphatase (ALP) through biotin-avidin interaction. The added 4-aminophenyl phosphate (4-APP) will hydrolyze to produce 4-aminophenol (4-AP) in the presence of ALP, which induces the reduction of silver ions into a silver shell. k) UV-vis absorption spectra of Au nanobipyramids under different amounts of 4-AP, 4-APP, and ALP. l) UV-vis absorption spectra of Au nanobipyramids with silver shells of different thicknesses induced by the reduction of silver nitrate with different concentrations of 4-AP. Reprinted with permission from ref.[187]; m) Scheme of colorimetric ELISA for ochratoxin A detection based on urease-induced metallization of Au nanoflowers. Reprinted with permission from ref.[188]

Transformation

The transformation of plasmonic nanostructures can also result in the changes in their optical properties. To develop colorimetric sensors based on this mechanism, core-shell plasmonic nanostructures are usually used. In most cases, the shell compositions of the core-shell nanostructures were altered by the analyte-induced transformation. For example, a number of methods were proposed for the detection of sulfides by utilizing the sulfidation of silver of Au@Ag core-shell nanostructures, leading to shell transformation from Ag to Ag₂S [191-194]. As displayed in Fig. 9a-c, in the presence of S²⁻, Ag₂S is formed on the surface of the Au@Ag nanocubes, which causes a dramatic redshift of spectrum covering most of the visible range of 500-750 nm, depending on the concentration of S²⁻due to the large difference between the refractive indexes of Ag (~0.05) and Ag₂S (~2.9) [193]. A colorimetric method for detecting S²⁻ was also developed based on the LSPR scattering change, which can be observed by dark-field microscopy (Fig. 9d-e) [194]. This method is highly sensitive because one can obtain the signal from an individual NP. Similarly, shell composition that changed from silver to silver iodide was designed for the detection of iodide [195].

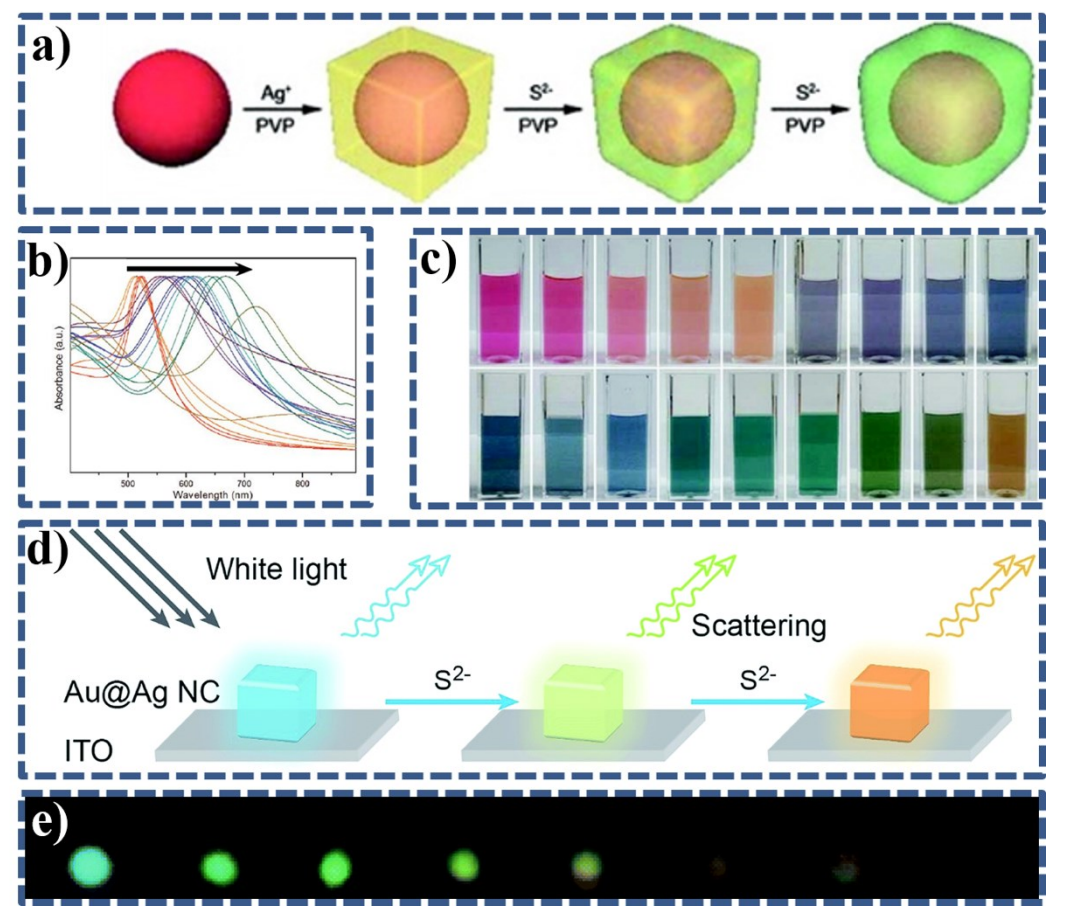


Figure 9. (a) Schematic illustration of the formation of Au@Ag/Ag₂S core-shell nanocubes (b) corresponding UV-vis spectra and (c) photographic images of Au seeds and Au@Ag core-shell nanocubes after the addition of increasing amounts of sulfide ions. Reprinted from ref. [193]with permission; (d) the scheme of sulfide ions-induced color changes on a single Au@Ag NC (e) dark-field images of Au@Ag nanocubes after reacting with different concentrations of NaHS. Reprinted from ref. [194]with permission

However, since the silver shell is not very stable, the selectivity of these methods based on Au@Ag core-shell nanostructures is not satisfactory. To overcome this limitation, Zeng *et al.* prepared Au/AgI dimeric nanoparticles for the colorimetric sensing of H₂S, which takes advantage of the chemical transformation of AgI to Ag₂S upon reacting with sulfide (Fig. 10) [196]. Such chemical transformation leads to a redshift of the plasmonic band of the attached Au nanoparticles, accompanied by a color change of the solution from purplish red to blue and finally to light green depending on the concentration of sulfide. This method is highly specific towards H₂S over other gas molecules since AgI is so a stable precipitate that very few interfering compounds can react with it.

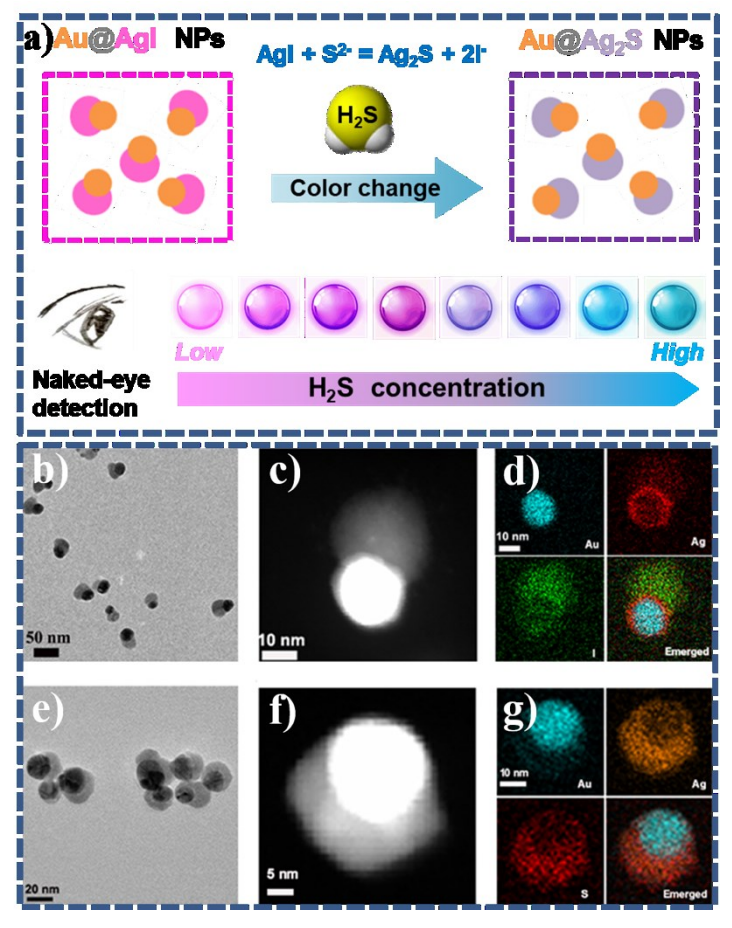


Figure 10. (a) Schematic illustration of the colorimetric sensing of hydrogen sulfide using Au@AgI dimeric nanoparticles (b) TEM, (c) STEM-HAADF and (d) EDX elemental maps of Au@AgI dimeric nanoparticles; (e) TEM, (f) STEM-HAADF and (g) EDX elemental maps of the products of the reaction between Au@AgI dimeric nanoparticles and S²-. Reprinted from ref. [196] with permission.

External stimuli

One of the most distinctive features of anisotropic plasmonic nanostructures is their orientation-dependent optical properties [197-199]. When anisotropic plasmonic nanostructures are bonded to counterparts with different functionalities, they are able to respond to a variety of external stimuli, mainly physical ones. In this subsection, we will discuss how these orientation-dependent optical properties of anisotropic plasmonic nanostructures can be utilized to develop more effective sensors by allowing instant selective excitation or quenching of specific plasmon modes. Physical stimuliresponsive optical changes have been used to develop a variety of devices, such as encryption devices, thermometers, stress sensors, and smart windows, *etc.*, which are

able to respond to different external stimuli such as light, heat, magnetic field, mechanical force, and electricity.

Optically responsive materials

Making light-responsive plasmonic nanostructure is of significant interest for its potential applications in many fields, since light is non-invasive and can be delivered instantaneously to a selected location [200]. As plasmonic nanostructures themselves are usually not light-responsive, strategies such as modifying them with surfactants that responses to light are widely used [200-208]. Upon the irradiation of light with certain wavelengths, those surfactants can be triggered to tune the optical properties of plasmonic nanostructures. On the other hand, embedding plasmonic nanostructures into a photo-responsive medium has been shown to tune the optical properties of the composite matrix by light irradiation. The above examples rely mainly on the photo-responsive ligands, which can change the interparticle distance among Au nanoparticles upon light irradiation through either affecting the dipole interaction among nanoparticles or forming covalent binding.

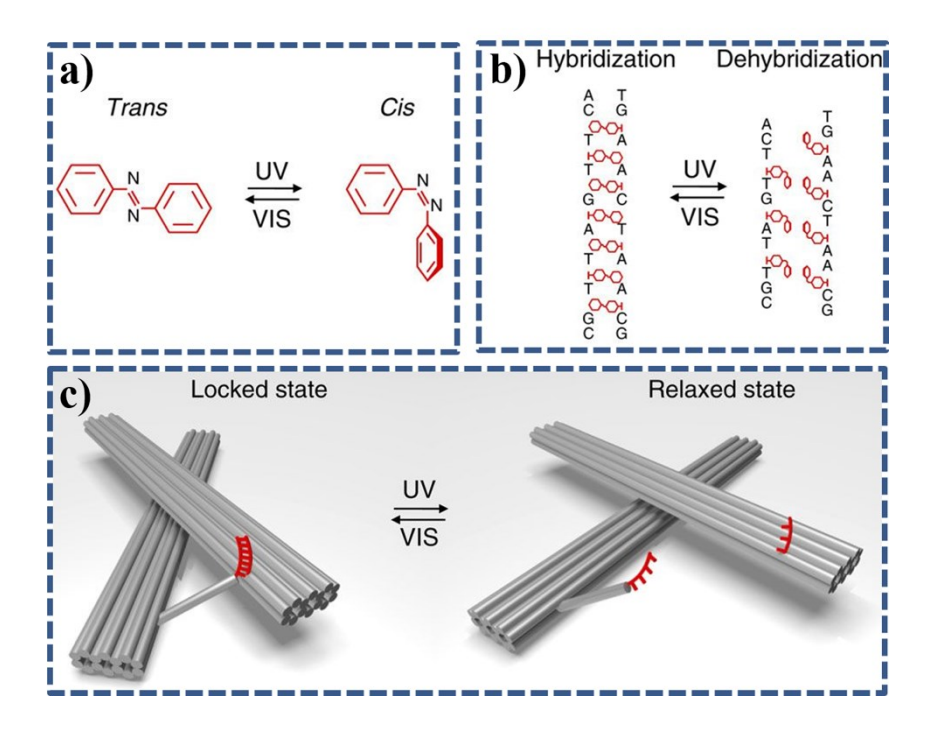


Figure 11. (a) *Trans–cis* photoisomerization of an azobenzene molecule by UV and visible light illumination. (b) Hybridization and dehybridization of azobenzene-modified DNA oligonucleotides controlled by *trans–cis* photoisomerization of azobenzene through UV and visible light illumination. (c) Photo-regulation of the DNA origami template between the locked and relaxed states by UV and visible light illumination. Reprinted from ref. [206] with permission.

Meanwhile, photo-responsive molecules that undergo reversible conformation changes can be also capped on plasmonic nanostructures to make them photo-responsive. Azobenzene is one of the most commonly used photoswitches, which undergoes a reversible conformation change from planar *trans* to the folded *cis* isomer under UV irradiation and switches back to the trans conformation under visible light radiation (Fig. 11a). By incorporating DNA origami with azobenzene, the linker DNA dehybridized because of the configuration change of azobenzene under UV irradiation (Fig. 11b), which relieves the mechanical strain. By attaching two gold nanorods on azobenzene-modified DNA origami, the angle between the two Au nanorods can be easily altered (Fig. 11c). This reversible orientation change between the two crossing Au nanorods results in circular dichroism changes in the visible-light range [206].

Besides the abovementioned strategies, the photothermal properties of plasmonic nanostructures [209, 210] can also make them photo-responsive. For example, Cu nanorods which were synthesized by a seeded growth method were embedded into polyvinyl alcohol to create photo-responsive films (Fig. 12) [211]. Upon irradiation with NIR, the temperature of Cu nanorods increased leading to the recovering of the photo-responsive film into its original shape [211]. Similarly, Au nanorods with different LSPR wavelengths can also be used to produce photo-responsive films, which can recover their original shapes upon irradiation with light with a wavelength of 530 and 860 nm, respectively [212]. Heat-responsive polymers were also used to obtain photo-responsive Au nanoparticles [204]. The photo-thermal properties of Au nanostructures under irradiation of different wavelengths can be used to develop an encryption film [213]. For example, under the irradiation of visible or NIR light, Au nanorods can generate heat patterns, which can be identified by thermal imaging infrared camera [213]. It should be noted that to tune the optical properties of plasmonic nanostructures based on photothermal effects, a laser with high-energy intensity is

usually required, which may initiate unexpected photochemical reactions, and even damage the structural integrity of the plasmonic nanostructures. However, this process seemed "disadvantage" was recently utilized to precisely assemble Au nanoparticles into chains [214]. On the other hand, plasmon-enhanced thermophoresis was demonstrated for the efficient assembly of Au nanotriangles at low optical power [215]. Au nanotriangles were capped with cetyltrimethylammonium chloride (CTAC) to get a hydrophilic and positive surface, which can head to the hot region on top of a plasmonic substrate due to the formation of the temperature gradient field. The thermophoresis-introduced electric force, electrostatic repulsive force, and van der Waals attraction enables the reversible assembly of plasmonic nanoparticles [215].

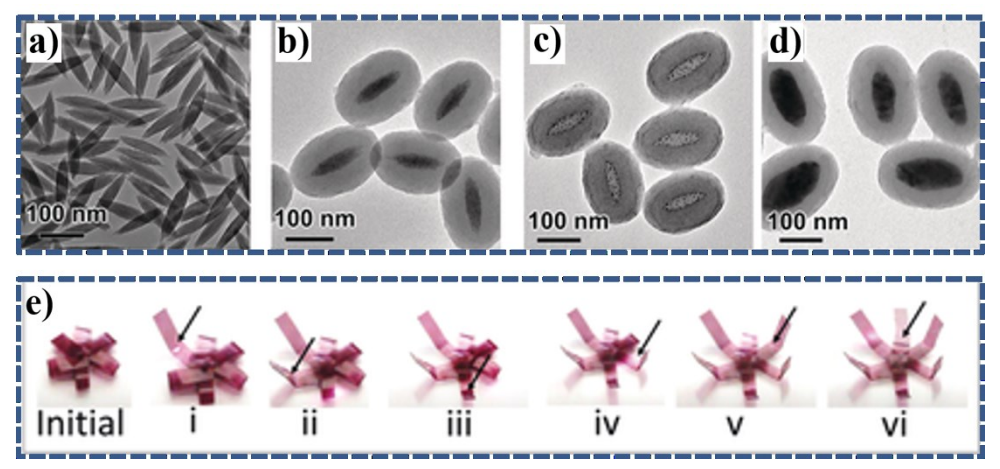


Figure 12. (a-d) Synthetic strategy for Cu nanorods, from (a) FeOOH to (b) FeOOH/Au nanoparticles, (c) Au-decorated resorcinol-formaldehyde capsules, and (d) Cu nanorods@ resorcinol-formaldehyde nanorods. (e) The composite film of Cu nanorods was deformed upon the NIR laser irradiation (980 nm). Reprinted from ref. [211] with permission.

Magnetically responsive materials

Magnetic tuning of plasmonic nanostructures is also of great interest for various applications, especially for analytical and biomedical ones [216]. As plasmonic nanomaterials are non-magnetic, a common strategy is to incorporate magnetic materials with them to obtain composite nanostructures. For example, Au nanorods were anchored on the surface of Fe₃O₄@SiO₂ nanorods in parallel to control the nanorod orientation by an external magnetic field [217]. As a result, the longitude or transverse mode of Au nanorods can be selectively excited [217]. More recently, a composite of Au microplates and γ-Fe₂O₃ nanoparticles was produced to magnetically

tune the optical properties of Au microplates [218]. In the absence of a magnetic field, the plate solution showed a shiny and golden color, while applying a magnetic field in parallel to the viewing direction, results in aligning the plates with the applied magnetic field, making the solution transparent due to the minimized cross-section of microplates [218]. A seeded-mediated growth method was also used to implant plasmonic rod-like structures vertically on magnetic nanoplates or nanorods [35]. These composites were fixed into a thin film with controllable orientation, which can exhibit polarization-dependent patterns for applications such as information encryption, as shown in Fig. 13 [35]. To produce composites of plasmonic nanostructures with magnetic counterparts, top-down methods such as lithographical [219] and electrochemical methods [220-222] were also used. These methods use templates to synthesize rod-like structures with both plasmonic properties and magnetic response, which can alter their optical properties by applying magnetic fields [219, 221]. It must be noted that besides magnetic metal or metal oxides materials, liquid crystals with magnetic response can also be used to create magnetically responsive plasmonic nanostructures [223].

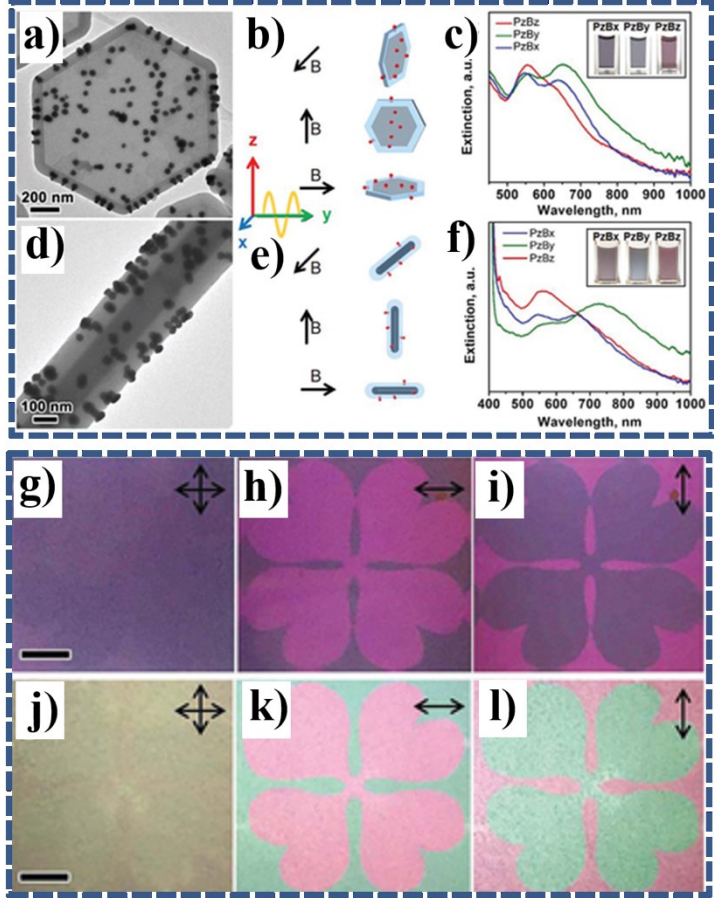


Figure 13. Magnetic tuning of (a-c) Au NP dimers on magnetic nanoplates and (d-f) Au NP dimers on magnetic rods. (g-l) By embedding the dimers on magnetic rods into a thin film, where their orientation was defined collectively using an external magnetic field, patterns of different polarizations can be produced. Reprinted from ref. [35] with permission.

Electrically responsive materials

Smart materials that can change their colors upon applying external voltages are of wide interest as electrochromic materials. While inorganic materials, such as WO₃, NiO, and V₂O₅, and organic materials, such as polyaniline and polypyrrole, are widely used for this purpose, they are suffering from limited color changes [224]. Alternatively, plasmonic nanostructures are used as electrochromic materials for their faster switching time, longer durability and wider spectral range [225]. The most common strategy is to control the deposition and dissolution of Ag on a substrate electrochemically [226-232]. Specifically, by sandwiching a gel electrolyte mainly containing silver nitrate and tetrabutylammonium bromide between a flat indium thin oxide (ITO) electrode and an ITO particle-modified electrode, the reduction from Ag⁺ to Ag can be achieved by applying an external voltage, resulting in a mirror state if Ag is deposited on the flat ITO electrode [226]. By reversing the external voltage, elemental Ag was deposited on the ITO particle-modified electrode, giving a dark state color. In the absence of an external voltage, the excess amount of Br can form a complex with Ag+, giving a transparent state of the device (Fig. 14) [226]. Similarly, by electrochemically controlling the transformation from CuCl₂, to CuCl, and to Cu, a reversible mirror device with transparent, blue, and mirror states was developed [233]. Later efforts using this silver deposition method mainly focused on the improvement of the mirror state or black state by modifying the electrodes [229, 231]. To achieve a stable mirror state even when electricity is unplugged, an ionic liquid was used to decrease the diffusion rate of bromide ions and thus the dissolution rate of metallic Ag [228].

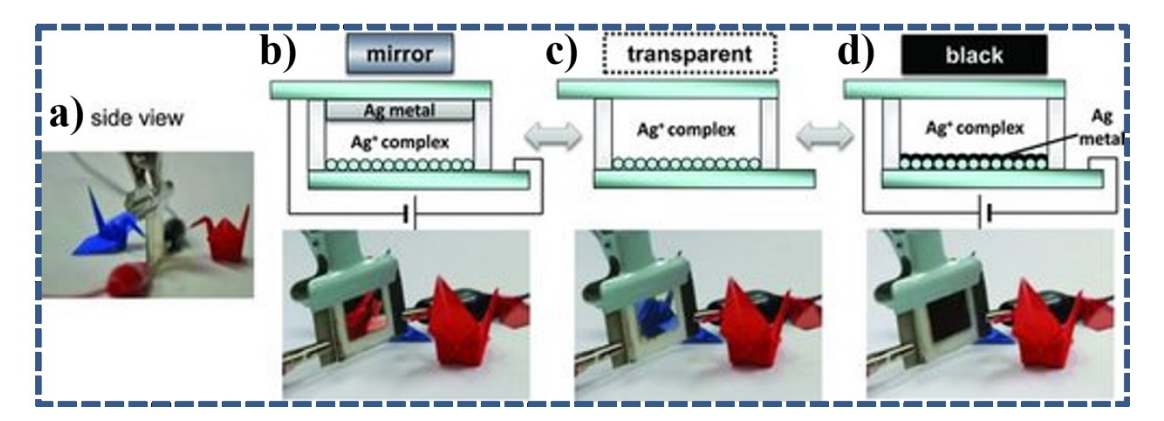


Figure 14. (a) Set-up of the electrochromic cell. By changing the external voltage, the cell demonstrated (b) mirror, (c) transparent, and (d) black states. Reprinted from ref. [226] with permission.

However, the above-mentioned demonstrations have limited spectrum ranges. To expand the spectrum range, electrochemical deposition of Ag should be carefully controlled to manipulate the size of deposited Ag particles on the electrode [227]. For example, by applying a step-wise external voltage, the nucleation and growth process of Ag nanoparticles can be controlled, and three primary colors, cyan, magenta, and yellow, were achieved [227] [226]. Controlling the aggregation of Ag nanoparticles to achieve a multicolor display under external voltage is another strategy [224]. More recently, electrochemical deposition of Ag on pre-synthesized and complex plasmonic nanostructure (hollow shell of Au/Ag alloy) has also demonstrated a multicolor display [232]. While with a polystyrene-patterned electrode, the deposition of Ag can result in full-color switching [230].

Conductive polymers are also employed to cap plasmonic nanostructures to make them electrically responsive [234]. For example, polyaniline (PANI), which changes its dielectric function when electrochemically switched between the oxidized and reduced states, has been used to modify Au NRs and Au nanobipyramids (Fig. 15 a and b)[235]. By depositing the PANI-capped Au nanostructures on an ITO substrate, an electrochemical cell that can show instant spectral changes was demonstrated (Fig. 15c). During the switch-on and -off processes, the extinction spectra of the PANI-capped Au nanostructures changed significantly. The PANI-caped Au NRs showed reversible peak shifts between 654 and 704 nm and peak intensities during the switching processes (Fig. 15 d and f). For the PANI-capped Au nanobipyramids, a broad peak at 800 nm was

observed at the oxidized state of PANI, which gradually red-shifted and decreased in intensity when the applied electrochemical potential was decreased (Fig. 15 e and g) [235]. Graphene [236, 237] and liquid crystals [238] as active surrounding media around plasmonic nanostructures have also been used to make them electrically responsive. Doping plasmonic elements into semiconductors to selectively control the transmission of NIR without affecting visible transparency, is a promising technique for energy-saving known as "smart windows" [239, 240]

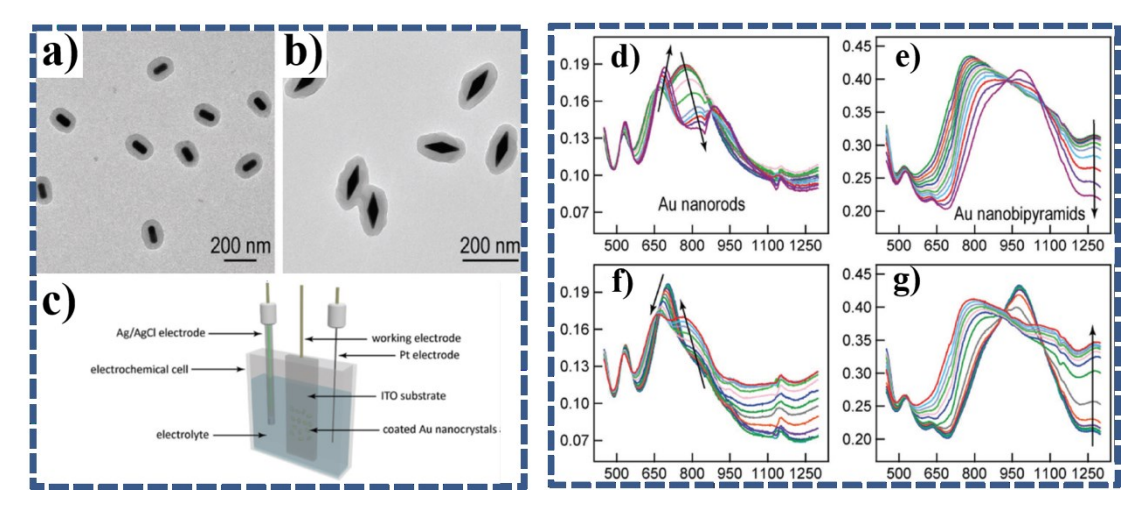


Figure 15. TEM images of (a) PANI-capped Au NRs and (b) PANI-capped Au nanobipyramids. (c) Schematic illustration of the three-electrode cell. By changing the external voltage, the extinction spectra of the plasmonic nanostructures changed during the switch-on (d and e) and switch-off (f and g) processes. Reprinted from ref. [235] with permission.

Other Stimuli

Anisotropic plasmonic nanostructures have also been used to develop materials that are responsive to other stimuli, such as pressure. For example, Au nanorods were embedded into a polymer matrix to create a stress sensor by taking advantage of its orientation-dependent optical properties. Upon applying pressure, the orientation of Au nanorods can be altered as demonstrated by the color change of the film [241]. Another anisotropic plasmonic nanostructure, Ag@Au nanoplates, was also used to make a stress-responsive film [242]. Thermo-responsive materials are also an interesting application of plasmonic nanostructures. Either temperature-sensitive medium or ligands have been used to make plasmonic nanostructures, mainly nanospheres, thermo-responsive[243-249].

Summary and Outlook

In summary, anisotropic plasmonic nanostructures offer broader tunability and higher sensitivity in LSPR properties than the isotropic ones, benefiting the development of colorimetric methods with enhanced sensitivity, a wider linear detection range, and a higher visual resolution. These advantages are particularly important for applications where the analyte concentration in the sample is ultralow. Because of the promising features of anisotropic plasmonic nanostructures-based colorimetric sensors, they have inspired a wide range of applications in environmental monitoring, food safety evaluation, molecular detections, clinical diagnostics, and smart materials. Despite the great achievement of this field, some challenges still need to be addressed. Firstly, compared to gold or silver nanospheres, the syntheses of most anisotropic plasmonic nanostructures are more complicated with lower production yield and less reproducibility. To overcome these limitations, more robust standardized protocols for the synthesis of anisotropic plasmonic nanostructures with higher production yield, simpler operation, and better reproducibility are highly desirable. Besides the anisotropic plasmonic nanostructures mentioned in this paper, other nanostructures such as nanoring [250], nanorattles [251], nanooctahedra [252], may also find their application in colorimetric sensing due to their unique optical properties. Secondly, the colorimetry always suffers from the difference in color recognition ability among different users and errors of light sources or background. The combination of suitable color picker software and APPs that are compatible with mobile devices (i.e. smartphone) would be an ideal way to solve the above-mentioned problems. Thirdly, effectively immobilizing the NP system into solid media will not only improve the portability but also will strengthen the stability and sensitivity of the sensors. Agarose gel is a good candidate for this purpose as it can decrease the risk of NP aggregation and facilitate the enrichment of analytes from the sample matrix [136, 196, 253, 254]. Lastly, how to design multi-channel sensing elements that are capable of detecting several analytes simultaneously is another challenge. For example, it is vital to detect

several kinds of pollutants in one analysis to better assess their environmental risks. Because anisotropic plasmonic nanostructures possess broadly tunable LSPR property and orientation-dependent features, they hold great promise for the design of multichannel colorimetric sensors. Artificial intelligence-aided statistical analyses would also help the development of multichannel colorimetric sensing when combined with its superb self-learning and data processing ability. Reusable smart materials that can return to their original states in controllable manners are desirable for practical applications, and their combination with a functional solid substrate represents a promising direction for future research.

Acknowledgements

This work was supported by the National Natural Science Foundation of China (81501521) and the Fundamental Research Funds for the Central Universities (18CX02037A). Y.Y. acknowledges the support from the U.S. National Science Foundation (CHE-1808788).

References

- [1] G. Yue, S. Su, N. Li, M. Shuai, X. Lai, D. Astruc, P. Zhao, Coord. Chem. Rev., 311 (2016) 75-84.
- [2] W. Chansuvarn, T. Tuntulani, A. Imyim, TrAC, Trends Anal. Chem., 65 (2015) 83-96.
- [3] E. Priyadarshini, N. Pradhan, Sens. Actuators, B:Chem., 238 (2017) 888-902.
- [4] X. Li, S. Zhang, Y. Dang, Z. Liu, Z. Zhang, D. Shan, X. Zhang, T. Wang, X. Lu, Anal. Chem., 91 (2019) 4031-4038.
- [5] P.G. Mahajan, N.C. Dige, B.D. Vanjare, S.-K. Hong, K.H. Lee, Sens. Actuators, B:Chem., 281 (2019) 720-729.
- [6] J. Sun, Y. Xianyu, X. Jiang, Chem. Soc. Rev., 43 (2014) 6239-6253.
- [7] J. Deng, P. Yu, Y. Wang, L. Yang, L. Mao, Adv. Mater., 26 (2014) 6933-6943.
- [8] T.M. Godoy-Reyes, A.M. Costero, P. Gaviña, R. Martínez-Máñez, F. Sancenón, ACS Appl. Nano Mater., 2 (2019) 1367-1373.
- [9] M. Iarossi, C. Schiattarella, I. Rea, L. De Stefano, R. Fittipaldi, A. Vecchione, R. Velotta, B.D. Ventura, ACS Omega, 3 (2018) 3805-3812.
- [10] F. Jia, Q. Liu, W. Wei, Z. Chen, Analyst, 144 (2019) 4865-4870.
- [11] C. C. Chang, C. P. Chen, T. H. Wu, C. H. Yang, C. W. Lin, C. Y. Chen, Nanomaterials, 9 (2019) 861.
- [12] B. Veigas, A. Matias, T. Calmeiro, E. Fortunato, A.R. Fernandes, P.V. Baptista, Analyst, 144 (2019) 3613-3619.
- [13] H. Kim, M. Park, J. Hwang, J.H. Kim, D. R. Chung, K. S. Lee, M. Kang, ACS Sens., 4 (2019) 1306-1312.
- [14] W. J. Chen, K. Kandasamy, Y. C. Chen, ACS Appl. Nano Mater., 2 (2019) 3348-3357.

- [15] D. Vilela, M.C. González, A. Escarpa, Anal. Chim. Acta, 751 (2012) 24-43.
- [16] L. Qin, G. Zeng, C. Lai, D. Huang, P. Xu, C. Zhang, M. Cheng, X. Liu, S. Liu, B. Li, H. Yi, Coord. Chem. Rev., 359 (2018) 1-31.
- [17] J. Du, L. Jiang, Q. Shao, X. Liu, R.S. Marks, J. Ma, X. Chen, Small, 9 (2013) 1467-1481.
- [18] H. Aldewachi, T. Chalati, M.N. Woodroofe, N. Bricklebank, B. Sharrack, P. Gardiner, Nanoscale, 10 (2018) 18-33.
- [19] H. Rao, X. Xue, H. Wang, Z. Xue, J. Mater. Chem. C, 7 (2019) 4610-4621.
- [20] H. Wang, H. Rao, M. Luo, X. Xue, Z. Xue, X. Lu, Coord. Chem. Rev., 398 (2019) 113003.
- [21] Z. Zhang, H. Wang, Z. Chen, X. Wang, J. Choo, L. Chen, Biosens. Bioelectron., 114 (2018) 52-65.
- [22] S.K. Kailasa, J.R. Koduru, M.L. Desai, T.J. Park, R.K. Singhal, H. Basu, TrAC, Trends Anal. Chem., 105 (2018) 106-120.
- [23] L. Tang, J. Li, ACS Sens., 2 (2017) 857-875.
- [24] X. Ma, S. He, B. Qiu, F. Luo, L. Guo, Z. Lin, ACS Sens., 4 (2019) 782-791.
- [25] Y. Xia, Anal. Bioanal. Chem., 408 (2016) 2813-2825.
- [26] Y. Peng, B. Xiong, L. Peng, H. Li, Y. He, E.S. Yeung, Anal. Chem., 87 (2015) 200-215.
- [27] L.M. Liz-Marzán, M. Grzelczak, Science, 356 (2017) 1120-1121.
- [28] H. E. Lee, H. Y. Ahn, J. Mun, Y. Y. Lee, M. Kim, N.H. Cho, K. Chang, W.S. Kim, J. Rho, K.T. Nam, Nature, 556 (2018) 360-365.
- [29] G. González-Rubio, P. Díaz-Núñez, A. Rivera, A. Prada, G. Tardajos, J. González-Izquierdo, L. Bañares, P. Llombart, L.G. Macdowell, M. Alcolea Palafox, L.M. Liz-Marzán, O. Peña-Rodríguez, A. Guerrero-Martínez, Science, 358 (2017) 640-644.
- [30] L. Chen, F. Ji, Y. Xu, L. He, Y. Mi, F. Bao, B. Sun, X. Zhang, Q. Zhang, Nano Lett., 14 (2014) 7201-7206.
- [31] M. Ha, J. H. Kim, M. You, Q. Li, C. Fan, J. M. Nam, Chem. Rev., 119 (2019) 12208-12278.
- [32] Y. Liu, X. Han, L. He, Y. Yin, Angew. Chem. Int. Ed., 51 (2012) 6373-6377.
- [33] W. Lewandowski, M. Fruhnert, J. Mieczkowski, C. Rockstuhl, E. Górecka, Nat. Commun., 6 (2015) 6590.
- [34] X. Han, Y. Liu, Y. Yin, Nano Lett., 14 (2014) 2466-2470.
- [35] J. Feng, F. Yang, X. Wang, F. Lyu, Z. Li, Y. Yin, Adv. Mater., 31 (2019) 1900789.
- [36] M. Wang, L. He, S. Zorba, Y. Yin, Nano Lett., 14 (2014) 3966-3971.
- [37] Z. Li, F. Yang, Y. Yin, Adv. Funct. Mater., 0 (2019) 1903467.
- [38] S. Barbosa, A. Agrawal, L. Rodriguez-Lorenzo, I. Pastoriza-Santos, R.A. Alvarez-Puebla, A. Kornowski, H. Weller, L.M. Liz-Marzan, Langmuir, 26 (2010) 14943-14950.
- [39] D.E. Charles, D. Aherne, M. Gara, D.M. Ledwith, Y.K. Gun'ko, J.M. Kelly, W.J. Blau, M.E. Brennan-Fournet, ACS Nano, 4 (2010) 55-64.
- [40] H. Chen, X. Kou, Z. Yang, W. Ni, J. Wang, Langmuir, 24 (2008) 5233-5237.
- [41] Y. Zhang, D.E. Charles, D.M. Ledwith, D. Aherne, S. Cunningham, M. Voisin, W.J. Blau, Y.K. Gun'ko, J.M. Kelly, M.E. Brennan-Fournet, RSC Adv., 4 (2014) 29022-29031.
- [42] S. Jayabal, A. Pandikumar, H.N. Lim, R. Ramaraj, T. Sun, N.M. Huang, Analyst, 140 (2015) 2540-2555.
- [43] H. Chen, L. Shao, Q. Li, J. Wang, Chem. Soc. Rev., 42 (2013) 2679-2724.
- [44] S.A. Alex, N. Chandrasekaran, A. Mukherjee, Anal. Methods, 8 (2016) 2131-2137.
- [45] C. Hamon, S. Novikov, L. Scarabelli, L. Basabe-Desmonts, L.M. Liz-Marzán, ACS Nano, 8 (2014) 10694-10703.
- [46] J. Wang, H.Z. Zhang, R.S. Li, C.Z. Huang, TrAC, Trends Anal. Chem., 80 (2016) 429-443.
- [47] T.K.S. Catherine J. Murphy, Anand M. Gole, Christopher J. Orendorff, J.X. Gao, L.F. Gou, Simona E.

- Hunyadi, T. Li, J. Phys. Chem. B, 109 (2005) 14017-14024.
- [48] C. Zhao, G. Wang, T. Takarada, X. Liang, M. Komiyama, M. Maeda, Colloids Surf. A, 568 (2019) 216-223.
- [49] I. Pastoriza-Santos, L.M. Liz-Marzán, J. Mater. Chem., 18 (2008) 1724-1737.
- [50] G. Wang, S. Tao, Y. Liu, L. Guo, G. Qin, K. Ijiro, M. Maeda, Y. Yin, Chem. Commun. (Camb), 52 (2016) 398-401.
- [51] J.S. DuChene, W. Niu, J.M. Abendroth, Q. Sun, W. Zhao, F. Huo, W.D. Wei, Chem. Mater., 25 (2013) 1392-1399.
- [52] J.E. Millstone, G.S. Métraux, C.A. Mirkin, Adv. Funct. Mater. 16 (2006) 1209-1214.
- [53] G. Wang, S. Tao, Y. Liu, L. Guo, G. Qin, K. Ijiro, M. Maeda, Y. Yin, Chem. Commun., 52 (2016) 398-401.
- [54] Y. Zhai, J.S. DuChene, Y.-C. Wang, J. Qiu, A.C. Johnston-Peck, B. You, W. Guo, B. DiCiaccio, K. Qian, E.W. Zhao, F. Ooi, D. Hu, D. Su, E.A. Stach, Z. Zhu, W.D. Wei, Nat. Mater., 15 (2016) 889-895.
- [55] S.D. Golze, R.A. Hughes, S. Rouvimov, R.D. Neal, T.B. Demille, S. Neretina, Nano Lett., 19 (2019) 5653-5660.
- [56] C. Gao, Z. Lu, Y. Liu, Q. Zhang, M. Chi, Q. Cheng, Y. Yin, Angew. Chem. Int. Ed. Engl., 51 (2012) 5629-5633.
- [57] Y. Zhang, L. Zhang, L. Wang, G. Wang, M. Komiyama, X. Liang, Microchim. Acta, 186 (2019) 713.
- [58] T.H. Chow, N. Li, X. Bai, X. Zhuo, L. Shao, J. Wang, Acc. Chem. Res, 52 (2019) 2136-2146.
- [59] Q. Li, X. Zhuo, S. Li, Q. Ruan, Q. H. Xu, J. Wang, Adv. Opt. Mater., 3 (2015) 801-812.
- [60] A. Campu, F. Lerouge, D. Chateau, F. Chaput, P. Baldeck, S. Parola, D. Maniu, A.M. Craciun, A. Vulpoi, S. Astilean, M. Focsan, Anal. Chem., 90 (2018) 8567-8575.
- [61] L. Vigderman, B.P. Khanal, E.R. Zubarev, Adv. Mater., 24 (2012) 4811-4841.
- [62] C.G. Khoury, T. Vo-Dinh, J. Phys. Chem. C, 112 (2008) 18849-18859.
- [63] L. Rodríguez-Lorenzo, R.A. Álvarez-Puebla, F.J.G. de Abajo, L.M. Liz-Marzán, J. Phys. Chem. C, 114 (2010) 7336-7340.
- [64] E. Nalbant Esenturk, A.R. Hight Walker, J. Raman Spectrose., 40 (2009) 86-91.
- [65] A.M. Fales, H. Yuan, T. Vo-Dinh, Langmuir, 27 (2011) 12186-12190.
- [66] S.K. Dondapati, T.K. Sau, C. Hrelescu, T.A. Klar, F.D. Stefani, J. Feldmann, ACS Nano, 4 (2010) 6318-6322.
- [67] M.A. Mahmoud, M.A. El-Sayed, J. Amer. Chem. Soc., 132 (2010) 12704-12710.
- [68] X. Lu, L. Au, J. McLellan, Z.-Y. Li, M. Marquez, Y. Xia, Nano Lett., 7 (2007) 1764-1769.
- [69] J. Zeng, M. Gong, D. Wang, M. Li, W. Xu, Z. Li, S. Li, D. Zhang, Z. Yan, Y. Yin, Nano Lett., 19 (2019) 3011-3018.
- [70] S.E. Skrabalak, J. Chen, Y. Sun, X. Lu, L. Au, C.M. Cobley, Y. Xia, Acc. Chem. Res, 41 (2008) 1587-1595.
- [71] Y. Sun, Y. Xia, Anal. Chem., 74 (2002) 5297-5305.
- [72] L. Zhang, J. Wang, J. Zhang, Y. Liu, L. Wu, J. Shen, Y. Zhang, Y. Hu, Q. Fan, W. Huang, L. Wang, ACS Sens., 2 (2017) 1435-1440.
- [73] Y. Tian, L. Zhang, J. Shen, L. Wu, H. He, D.-L. Ma, C.-H. Leung, W. Wu, Q. Fan, W. Huang, L. Wang, Small, 12 (2016) 2913-2920.
- [74] X. Wu, T. Ming, X. Wang, P. Wang, J. Wang, J. Chen, ACS Nano, 4 (2010) 113-120.
- [75] C. Noguez, J. Phys. Chem. C, 111 (2007) 3806-3819.
- [76] C. Deeb, X. Zhou, R. Miller, S.K. Gray, S. Marguet, J. Plain, G.P. Wiederrecht, R. Bachelot, J. Phys. Chem. C, 116 (2012) 24734-24740.

- [77] D. Lee, S. Yoon, J. Phys. Chem. C, 119 (2015) 7873-7882.
- [78] P.S. Teo, P. Rameshkumar, A. Pandikumar, Z.-T. Jiang, M. Altarawneh, N.M. Huang, Microchim. Acta, 184 (2017) 4125-4132.
- [79] S. Bamrungsap, J. Cherngsuwanwong, P. Srisurat, J. Chonirat, N. Sangsing, N. Wiriyachaiporn, Anal. Methods, 11 (2019) 1387-1392.
- [80] N. Priyadarshni, P. Nath, Nagahanumaiah, N. Chanda, ACS Sustain. Chem. Eng., 6 (2018) 6264-6272.
- [81] X. Zhou, C. Xu, Y. Jin, B. Li, Spectrochim. Acta A, 223 (2019) 117263.
- [82] L. Zhang, Y. Huang, J. Wang, Y. Rong, W. Lai, J. Zhang, T. Chen, Langmuir, 31 (2015) 5537-5544.
- [83] J. Du, H. Singh, W.J. Dong, Y.H. Bai, T.H. Yi, Sens. Actuators, B:Chem., 265 (2018) 285-292.
- [84] J. Du, L. Jiang, Q. Shao, X. Liu, R.S. Marks, J. Ma, X. Chen, Small, 9 (2013) 1467-1481.
- [85] N. Xiao, C. Yu, Anal. Chem., 82 (2010) 3659-3663.
- [86] L. Qi, Y. Shang, F. Wu, Microchim. Acta, 178 (2012) 221-227.
- [87] Y. Zhou, H. Zhao, C. Li, P. He, W. Peng, L. Yuan, L. Zeng, Y. He, Talanta, 97 (2012) 331-335.
- [88] H. Lee, H.K. Sung, C. Park, Y. Kim, J. Ind. Eng. Chem., 48 (2017) 235-241.
- [89] H.K. Sung, S.Y. Oh, C. Park, Y. Kim, Langmuir, 29 (2013) 8978-8982.
- [90] T. Kiatkumjorn, P. Rattanarat, W. Siangproh, O. Chailapakul, N. Praphairaksit, Talanta, 128 (2014) 215-220.
- [91] Z. Chen, T. Lou, Q. Wu, K. Li, L. Tan, J. Sun, Sens. Actuators, B:Chem., 221 (2015) 365-369.
- [92] S. Kaviya, E. Prasad, Anal. Methods, 7 (2015) 168-174.
- [93] Y. Tian, Q. Liu, Y. Jiao, R. Jia, Z. Chen, Mikrochim. Acta, 185 (2017) 6.
- [94] G. Song, F. Zhou, C. Xu, B. Li, Analyst, 141 (2016) 1257-1265.
- [95] M. Zhang, B.-C. Ye, Anal. Chem., 83 (2011) 1504-1509.
- [96] J. Wei, Y. Guo, J. Li, M. Yuan, T. Long, Z. Liu, Anal. Chem., 89 (2017) 9781-9787.
- [97] L. Zhang, C. Xu, G. Song, B. Li, RSC Adv., 5 (2015) 27003-27008.
- [98] Y. Wang, X. Zhou, C. Xu, Y. Jin, B. Li, Sci. Rep., 8 (2018) 5296.
- [99] C. Liu, B. Li, C. Xu, Microchim. Acta, 181 (2014) 1407-1413.
- [100] J. Tashkhourian, M. Afsharinejad, A.R. Zolghadr, Sens. Actuators, B:Chem., 232 (2016) 52-59.
- [101] M. Zhu, H. Qian, X. Meng, S. Jin, Z. Wu, R. Jin, Nano Lett., 11 (2011) 3963-3969.
- [102] X. Liu, I.P. Hamilton, J. Amer. Chem. Soc., 136 (2014) 17757-17761.
- [103] H. Yuan, C.G. Khoury, H. Hwang, C.M. Wilson, G.A. Grant, T. Vo-Dinh, Nanotechnology, 23 (2012) 075102.
- [104] L. Shao, A.S. Susha, L.S. Cheung, T.K. Sau, A.L. Rogach, J. Wang, Langmuir, 28 (2012) 8979-8984.
- [105] M.S. Verma, P.Z. Chen, L. Jones, F.X. Gu, RSC Adv., 4 (2014) 10660-10668.
- [106] M.S. Verma, P.Z. Chen, L. Jones, F.X. Gu, Biosens. Bioelectron., 61 (2014) 386-390.
- [107] A. Rajeshwari, D. Karthiga, N. Chandrasekaran, A. Mukherjee, Mater. Sci. Eng., C, 67 (2016) 711-716.
- [108] Q. Wang, Y. Li, M. Li, C. Wen, R. Liu, F. Subhan, Z. Yan, J. Zeng, Anal. Methods, 7 (2015) 6837-6841.
- [109] N. Ding, H. Zhao, W. Peng, Y. He, Y. Zhou, L. Yuan, Y. Zhang, Colloids Surf. A, 395 (2012) 161-167.
- [110] Y. He, X. Zhang, Sens. Actuators, B:Chem., 222 (2016) 320-324.
- [111] N. Bi, J. Xu, L. Jia, Microchim. Acta, 184 (2017) 3961-3967.
- [112] C. Xu, L. Lan, Y. Yao, J. Ping, Y. Li, Y. Ying, Sens. Actuators B: Chem., 273 (2018) 642-648.
- [113] Z. Sun, W. Ni, Z. Yang, X. Kou, L. Li, J. Wang, Small, 4 (2008) 1287-1292.
- [114] L. Wang, Y. Zhu, L. Xu, W. Chen, H. Kuang, L. Liu, A. Agarwal, C. Xu, N.A. Kotov, Angew. Chem. Int. Ed., 49 (2010) 5472-5475.

- [115] L. Lu, Y. Xia, Anal. Chem., 87 (2015) 8584-8591.
- [116] L. Chen, L. Lu, S. Wang, Y. Xia, ACS Sens., 2 (2017) 781-788.
- [117] J. Wang, P. Zhang, C.M. Li, Y.F. Li, C.Z. Huang, Biosens. Bioelectron., 34 (2012) 197-201.
- [118] L. Chang, Y. Khan, L. Li, N. Yang, P. Yin, L. Guo, RSC Adv., 7 (2017) 13896-13903.
- [119] F. Zhang, J. Zhu, J. J. Li, J. W. Zhao, J. Mater. Chem. C, 3 (2015) 6035-6045.
- [120] J. Guan, Y.C. Wang, S. Gunasekaran, J Food Sci., 80 (2015) N828-N833.
- [121] T. Lin, M. Zhang, F. Xu, X. Wang, Z. Xu, L. Guo, Sens. Actuators, B: Chem., 261 (2018) 379-384.
- [122] Q. Chen, T. Lin, J. Huang, Y. Chen, L. Guo, F. Fu, Anal. Methods, 10 (2018) 504-507.
- [123] R. Yang, D. Song, C. Wang, A. Zhu, R. Xiao, J. Liu, F. Long, RSC Adv., 5 (2015) 102542-102549.
- [124] E. Detsri, Chin. Chem. Lett., 27 (2016) 1635-1640.
- [125] A. Apilux, W. Siangproh, N. Praphairaksit, O. Chailapakul, Talanta, 97 (2012) 388-394.
- [126] J. Zhu, T.T. Jia, J.J. Li, X. Li, J.W. Zhao, Spectrochim. Acta A, 207 (2019) 337-347.
- [127] P. Nalawade, S. Kapoor, Spectrochim. Acta A, 116 (2013) 132-135.
- [128] W. Siangproh, O. Chailapakul, K. Songsrirote, Talanta, 153 (2016) 197-202.
- [129] S.A. Alex, N. Chandrasekaran, A. Mukherjee, J. Mol. Liq., 264 (2018) 119-126.
- [130] Y. Ma, Y. Zhu, B. Liu, G. Quan, L. Cui, Materials (Basel), 11 (2018) 1629.
- [131] X. Li, X. Lin, S. Lin, X. Sun, D. Gao, B. Liu, H. Zhao, J. Zhang, S. Cong, L. Wang, ACS Appl. Nano Mater., 2 (2019) 3161-3168.
- [132] T. Sasikumar, M. Ilanchelian, Anal. Methods, 9 (2017) 3151-3158.
- [133] Z. Chen, Z. Zhang, C. Qu, D. Pan, L. Chen, Analyst, 137 (2012) 5197-5200.
- [134] X. Zhu, C. Liu, J. Liu, Int. J. Anal. Chem., 2019 (2019) 8961837.
- [135] J. Zhu, Y. Q. Yu, J. J. Li, J. W. Zhao, RSC Adv., 6 (2016) 25611-25619.
- [136] J. B. Zeng, Y. Y. Cao, J. J. Chen, X. D. Wang, J. F Yu, B. B. Yu, Z. F. Yan, X. Chen, Nanoscale, 6 (2014) 9939-9943.
- [137] Y. Li, Q. Wang, X. Zhou, C. Y. Wen, J. Yu, X. Han, X. Li, Z. F. Yan, J. Zeng, Sens. Actuators, B:Chem., 228 (2016) 366-372.
- [138] S. Lee, Y. S. Nam, S.-H. Choi, Y. Lee, K. B. Lee, Microchim. Acta, 183 (2016) 3035-3041.
- [139] A. Yakoh, P. Rattanarat, W. Siangproh, O. Chailapakul, Talanta, 178 (2018) 134-140.
- [140] X. Hou, S. Chen, J. Tang, Y. Xiong, Y. Long, Anal. Chim. Acta, 825 (2014) 57-62.
- [141] Z. Zhang, Z. Chen, F. Cheng, Y. Zhang, L. Chen, Biosens. Bioelectron., 89 (2017) 932-936.
- [142] X. Cheng, Y. Huang, C. Yuan, K. Dai, H. Jiang, J. Ma, Sens. Actuators B: Chem., 282 (2019) 838-843.
- [143] Z. Zhang, Z. Chen, F. Cheng, Y. Zhang, L. Chen, Analyst, 141 (2016) 2955-2961.
- [144] Z. Zhang, Z. Chen, L. Chen, Langmuir, 31 (2015) 9253-9259.
- [145] Q. Zhong, Y. Chen, X. Qin, Y. Wang, C. Yuan, Y. Xu, Mikrochim. Acta, 186 (2019) 161.
- [146] X. Ma, Y. Lin, L. Guo, B. Qiu, G. Chen, H.H. Yang, Z. Lin, Biosens. Bioelectron., 87 (2017) 122-128.
- [147] Y. Lin, M. Zhao, Y. Guo, X. Ma, F. Luo, L. Guo, B. Qiu, G. Chen, Z. Lin, Sci. Rep., 6 (2016) 37879.
- [148] Y. Liu, J. Wang, C. Zhao, X. Guo, X. Song, W. Zhao, S. Liu, K. Xu, J. Li, Anal. Chim. Acta, 1048 (2019) 154-160.
- [149] Y. Xiong, K. Pei, Y. Wu, H. Duan, W. Lai, Y. Xiong, Sens. Actuators, B: Chem., 267 (2018) 320-327.
- [150] H. Yang, A. Liu, M. Wei, Y. Liu, B. Lv, W. Wei, Y. Zhang, S. Liu, Anal. Chem., 89 (2017) 12094-12100.
- [151] Y. Gu, J. Song, M.X. Li, T.T. Zhang, W. Zhao, J.J. Xu, M. Liu, H.Y. Chen, Anal. Chem., 89 (2017) 10585-10591.
- [152] L. Saa, M. Coronado-Puchau, V. Pavlov, L.M. Liz-Marzán, Nanoscale, 6 (2014) 7405-7409.
- [153] Z. Chen, C. Zhang, Q. Wu, K. Li, L. Tan, Sens. Actuators, B:Chem., 220 (2015) 314-317.

- [154] R.K. Bera, C.R. Raj, J. Photochem. Photobiol, A: Chem., 270 (2013) 1-6.
- [155] S. Liu, X. Li, Mater. Sci. Eng. B, 240 (2019) 49-54.
- [156] F. Cheng, Z. Chen, Z. Zhang, L. Chen, Analyst, 141 (2016) 1918-1921.
- [157] S. Lu, X. Zhang, L. Chen, P. Yang, Microchim. Acta, 185 (2017) 76.
- [158] Z. Zhang, Z. Chen, D. Pan, L. Chen, Langmuir, 31 (2014) 643-650.
- [159] Z. Zhang, Z. Chen, S. Wang, F. Cheng, L. Chen, ACS Appl. Mater. Interfaces, 7 (2015) 27639-27645.
- [160] M. Liu, P. Guyot-Sionnest, T. W. Lee, S.K. Gray, Phys. Rev. B, 76 (2007) 235428.
- [161] Y. Lin, S. Xu, J. Yang, Y. Huang, Z. Chen, B. Qiu, Z. Lin, G. Chen, L. Guo, Sens. Actuators B: Chem., 267 (2018) 502-509.
- [162] D. Yuan, J.J. Liu, H.H. Yan, C.M. Li, C.Z. Huang, J. Wang, Talanta, 203 (2019) 220-226.
- [163] S. Lu, X. Zhang, L. Chen, P. Yang, Sens. Actuators B: Chem., 259 (2018) 1066-1072.
- [164] Y. Wang, R. Liang, W. Liu, Q. Zhao, X. Zhu, L. Yang, P. Zou, X. Wang, F. Ding, H. Rao, Sens. Actuators B: Chem., 273 (2018) 1627-1634.
- [165] Z. Chen, C. Chen, H. Huang, F. Luo, L. Guo, L. Zhang, Z. Lin, G. Chen, Anal. Chem., 90 (2018) 6222-6228.
- [166] L. Chen, M. Lin, P. Yang, New J.Chem., 43 (2019) 10841-10849.
- [167] L. Saa, R. Grinyte, A. Sanchez-Iglesias, L.M. Liz-Marzan, V. Pavlov, ACS Appl. Mater. Interfaces, 8 (2016) 11139-11146.
- [168] S.Wu, D.D. Li, Z.M. Gao, J.M. Wang, Microchim. Acta, 184 (2017) 4383-4391.
- [169] Y. Liu, B. Lv, A. Liu, G. Liang, L. Yin, Y. Pu, W. Wei, S. Gou, S. Liu, Sens. Actuators B: Chem., 265 (2018) 675-681.
- [170] G. Weng, X. Zhao, J. Zhao, J. Li, J. Zhu, J. Zhao, Sens. Actuators, B:Chem., 299 (2019) 126982.
- [171] S. Wang, Z. Chen, L. Chen, R. Liu, L. Chen, Analyst, 138 (2013) 2080-2084.
- [172] Y. Li, G. Luo, Z. Qing, X. Li, Z. Zou, R. Yang, Microchim. Acta, 186 (2019) 565.
- [173] X. Fang, H. Ren, H. Zhao, Z. Li, Microchim. Acta, 184 (2016) 415-421.
- [174] Y. Zhou, W. Huang, Y. He, Sens. Actuators, B:Chem., 270 (2018) 187-191.
- [175] T. Cai, Y. Gao, J. Yan, Y. Wu, J. Di, RSC Adv., 7 (2017) 29122-29128.
- [176] K. Tan, G. Yang, H. Chen, P. Shen, Y. Huang, Y. Xia, Biosens. Bioelectron., 59 (2014) 227-232.
- [177] S. Jafarinejad, M. Ghazi-Khansari, F. Ghasemi, P. Sasanpour, M.R. Hormozi-Nezhad, Sci. Rep., 7 (2017) 8266.
- [178] J. M. Lin, Y. Q. Huang, Z. b. Liu, C. Q. Lin, X. Ma, J. M. Liu, RSC Adv., 5 (2015) 99944-99950.
- [179] W. Duan, A. Liu, Q. Li, Z. Li, C.Y. Wen, Z. Cai, S. Tang, X. Li, J. Zeng, Analyst, 144 (2019) 4582-4588.
- [180] T. Lin, Z. Li, Z. Song, H. Chen, L. Guo, F. Fu, Z. Wu, Talanta, 148 (2016) 62-68.
- [181] T. Lin, Y. Wu, Z. Li, Z. Song, L. Guo, F. Fu, Anal. Chem., 88 (2016) 11022-11027.
- [182] N. Fahimi-Kashani, P. Shadabipour, M.R. Hormozi-Nezhad, RSC Adv., 5 (2015) 82906-82915.
- [183] C. Dwivedi, A. Chaudhary, A. Gupta, C.K. Nandi, ACS Appl. Mater. Interfaces, 7 (2015) 5039-5044.
- [184] Y. Qi, J. Zhao, G. J. Weng, J. J. Li, X. Li, J. Zhu, J. W. Zhao, J. Mater. Chem. C, 6 (2018) 12283-12293.
- [185] X. Yang, Z. Gao, Chem. Commun. (Camb), 51 (2015) 6928-6931.
- [186] Y. Li, X. Ma, Z. Xu, M. Liu, Z. Lin, B. Qiu, L. Guo, G. Chen, Analyst, 141 (2016) 2970-2976.
- [187] S. Xu, W. Ouyang, P. Xie, Y. Lin, B. Qiu, Z. Lin, G. Chen, L. Guo, Anal. Chem., 89 (2017) 1617-1623.
- [188] K. Pei, Y. Xiong, B. Xu, K. Wu, X. Li, H. Jiang, Y. Xiong, Sens. Actuators, B:Chem., 262 (2018) 102-109.
- [189] H. Zhang, S. Wu, L. Zhang, L. Jiang, F. Huo, D. Tian, Anal. Methods, 11 (2019) 2286-2291.
- [190] J. Chen, A.A. Jackson, V.M. Rotello, S.R. Nugen, Small, 12 (2016) 2469-2475.

- [191] B. Xiong, R. Zhou, J. Hao, Y. Jia, Y. He, E.S. Yeung, Nat. Commun., 4 (2013) 1708.
- [192] H. Huang, Q. Li, J. Wang, Z. Li, X. F. Yu, P.K. Chu, Plasmonics, 9 (2013) 11-16.
- [193] G. Park, C. Lee, D. Seo, H. Song, Langmuir, 28 (2012) 9003-9009.
- [194] L. Zhang, J. Zhang, F. Wang, J. Shen, Y. Zhang, L. Wu, X. Lu, L. Wang, Q. Fan, W. Huang, RSC Adv., 8 (2018) 5792-5796.
- [195] Y. Qi, J. Zhu, J. J. Li, J. W. Zhao, Sens. Actuators B: Chem., 253 (2017) 612-620.
- [196] J. Zeng, M. Li, A. Liu, F. Feng, T. Zeng, W. Duan, M. Li, M. Gong, C. Y. Wen, Y. Yin, Adv. Funct. Mater., 28 (2018) 1800515.
- [197] L. Guo, Y. Xu, A.R. Ferhan, G. Chen, D.-H. Kim, J. Amer. Chem. Soc., 135 (2013) 12338-12345.
- [198] Z. Li, M. Wang, X. Zhang, D. Wang, W. Xu, Y. Yin, Nano Lett., 19 (2019) 6673-6680.
- [199] Z. Li, F. Yang, Y. Yin, Adv. Funct. Mater., 30 (2020) 1903467.
- [200] Y. Shiraishi, K. Tanaka, E. Shirakawa, Y. Sugano, S. Ichikawa, S. Tanaka, T. Hirai, Angew. Chem. Int. Ed., 52 (2013) 8304-8308.
- [201] R. Klajn, K.J.M. Bishop, B.A. Grzybowski, Proc. Natl. Acad. Sci., 104 (2007) 10305-10309.
- [202] Y. Shiraishi, E. Shirakawa, K. Tanaka, H. Sakamoto, S. Ichikawa, T. Hirai, ACS Appl. Mater. Interfaces, 6 (2014) 7554-7562.
- [203] P.K. Kundu, D. Samanta, R. Leizrowice, B. Margulis, H. Zhao, M. Börner, T. Udayabhaskararao, D. Manna, R. Klajn, Nat. Chem., 7 (2015) 646-652.
- [204] T. Ding, V.K. Valev, A.R. Salmon, C.J. Forman, S.K. Smoukov, O.A. Scherman, D. Frenkel, J.J. Baumberg, Proc. Natl. Acad. Sci., 113 (2016) 5503-5507.
- [205] H. He, M. Feng, Q. Chen, X. Zhang, H. Zhan, Angew. Chem. Int. Ed., 55 (2016) 936-940.
- [206] A. Kuzyk, Y. Yang, X. Duan, S. Stoll, A.O. Govorov, H. Sugiyama, M. Endo, N. Liu, Nat. Commun., 7 (2016) 10591.
- [207] Y. Chen, Z. Wang, Y. He, Y.J. Yoon, J. Jung, G. Zhang, Z. Lin, Proc. Natl. Acad. Sci., 115 (2018) E1391-E1400.
- [208] A. Manna, P.-L. Chen, H. Akiyama, T.-X. Wei, K. Tamada, W. Knoll, Chem. Mater., 15 (2003) 20-28.
- [209] D. Wang, S.C. Pillai, S.-H. Ho, J. Zeng, Y. Li, D.D. Dionysiou, Appl. Catal. B, Environ., 237 (2018) 721-741.
- [210] S. Link, C. Burda, B. Nikoobakht, M.A. El-Sayed, J.Phys. Chem. B, 104 (2000) 6152-6163.
- [211] J. Chen, J. Feng, F. Yang, R. Aleisa, Q. Zhang, Y. Yin, Angew. Chem. Int. Ed., 58 (2019) 9275-9281.
- [212] S.R. Mishra, J.B. Tracy, ACS Appl. Nano Mater., 1 (2018) 3063-3067.
- [213] H. Kang, J.W. Lee, Y. Nam, ACS Appl. Mater. Interfaces, 10 (2018) 6764-6771.
- [214] L.O. Herrmann, V.K. Valev, C. Tserkezis, J.S. Barnard, S. Kasera, O.A. Scherman, J. Aizpurua, J.J. Baumberg, Nat. Commun., 5 (2014) 4568.
- [215] L. Lin, X. Peng, M. Wang, L. Scarabelli, Z. Mao, L.M. Liz-Marzan, M.F. Becker, Y. Zheng, ACS Nano, 10 (2016) 9659-9668.
- [216] Q. Zhang, J. Ge, J. Goebl, Y. Hu, Y. Sun, Y. Yin, Adv. Mater, 22 (2010) 1905-1909.
- [217] M. Wang, C. Gao, L. He, Q. Lu, J. Zhang, C. Tang, S. Zorba, Y. Yin, J. Am. Chem Soc., 135 (2013) 15302-15305.
- [218] J. Goebl, Y. Liu, S. Wong, S. Zorba, Y. Yin, Nanoscale Horiz., 1 (2016) 64-68.
- [219] M. Zhang, D.J. Magagnosc, I. Liberal, Y. Yu, H. Yun, H. Yang, Y. Wu, J. Guo, W. Chen, Y.J. Shin, A. Stein, J.M. Kikkawa, N. Engheta, D.S. Gianola, C.B. Murray, C.R. Kagan, Nat. Nanotechnol., 12 (2016) 228-232.
- [220] I. Jung, H. Yoo, H.-J. Jang, S. Cho, K. Lee, S. Hong, S. Park, Angew. Chem. Int. Ed., 57 (2018) 1841-

- 1845.
- [221] R. Geryak, J. Geldmeier, K. Wallace, V.V. Tsukruk, Nano Lett., 15 (2015) 2679-2684.
- [222] I. Jung, S. Ih, H. Yoo, S. Hong, S. Park, Nano Lett., 18 (2018) 1984-1992.
- [223] Q. Liu, Y. Cui, D. Gardner, X. Li, S. He, I.I. Smalyukh, Nano Lett., 10 (2010) 1347-1353.
- [224] Z. He, X. Yuan, Q. Wang, L. Yu, C. Zou, C. Li, Y. Zhao, B. He, L. Zhang, H. Zhang, H. Yang, Adv. Opt.Mater., 4 (2016) 106-111.
- [225] A. Cannavale, P. Cossari, G.E. Eperon, S. Colella, F. Fiorito, G. Gigli, H.J. Snaith, A. Listorti, Energ. Environ. Sci., 9 (2016) 2682-2719.
- [226] S. Araki, K. Nakamura, K. Kobayashi, A. Tsuboi, N. Kobayashi, Adv. Mater., 24 (2012) 122-126.
- [227] A. Tsuboi, K. Nakamura, N. Kobayashi, Chem. Mater., 26 (2014) 6477-6485.
- [228] C. Park, S. Seo, H. Shin, B.D. Sarwade, J. Na, E. Kim, Chem. Sci., 6 (2015) 596-602.
- [229] K.R. Jeong, I. Lee, J.Y. Park, C.S. Choi, S. H. Cho, J.L. Lee, Npg Asia Mater., 9 (2017) 362.
- [230] C. Park, J. Na, M. Han, E. Kim, ACS Nano, 11 (2017) 6977-6984.
- [231] M. Qiu, P. Sun, B. Zhang, J. Yu, Y. Fu, X. Yu, C. Zhao, W. Mai, Adv. Opt. Mater., 6 (2018) 1800338.
- [232] N. Li, P. Wei, L. Yu, J. Ji, J. Zhao, C. Gao, Y. Li, Y. Yin, Small, 15 (2019) 1804974.
- [233] A.L. S. Eh, M. F. Lin, M. Cui, G. Cai, P.S. Lee, J. Mater. Chem. C, 5 (2017) 6547-6554.
- [234] Y. Leroux, J.C. Lacroix, C. Fave, G. Trippe, N. Fé lidj, J. Aubard, A. Hohenau, and J. R. Krenn, ACS Nano, 2 (2008) 728-732.
- [235] W. Lu, N. Jiang, J. Wang, Adv. Mater., 29 (2017)1604862.
- [236] Y. Yao, M.A. Kats, P. Genevet, N. Yu, Y. Song, J. Kong, F. Capasso, Nano Lett., 13 (2013) 1257-1264.
- [237] J. Kim, H. Son, D.J. Cho, B. Geng, W. Regan, S. Shi, K. Kim, A. Zettl, Y.R. Shen, F. Wang, Nano Lett, 12 (2012) 5598-5602.
- [238] S. Khatua, W.S. Chang, P. Swanglap, J. Olson, S. Link, Nano Lett, 11 (2011) 3797-3802.
- [239] G. Garcia, R. Buonsanti, E.L. Runnerstrom, R.J. Mendelsberg, A. Llordes, A. Anders, T.J. Richardson, D.J. Milliron, Nano Lett., 11 (2011) 4415-4420.
- [240] E.L. Runnerstrom, A. Llordés, S.D. Lounis, D.J. Milliron, Chem. Commun., 50 (2014) 10555-10572.
- [241] L. Fu, Y. Liu, W. Wang, M. Wang, Y. Bai, E.L. Chronister, L. Zhen, Y. Yin, Nanoscale, 7 (2015) 14483-14488.
- [242] L. S. Fu, W. S. Wang, C. Y. Xu, Y. Li, L. Zhen, Sci. Rep., 7 (2017) 1676.
- [243] Y. Liu, X. Han, L. He, Y. Yin, Angew. Chem. Int. Ed. Engl., 51 (2012) 6373-6377.
- [244] K. Heo, C. Miesch, T. Emrick, R.C. Hayward, Nano Lett., 13 (2013) 5297-5302.
- [245] K. L. Hamner, C. M. Alexander, K. Coopersmith, D. Reishofer, C. Provenza, M.M. Maye, ACS Nano, 7 (2013) 7011-7020.
- [246] F. Han, S.R.C. Vivekchand, A.H. Soeriyadi, Y. Zheng, J.J. Gooding, Nanoscale, 10 (2018) 4284-4290.
- [247] A.W.R. Tao Ding, Lars O. Herrmann, Vladimir Turek and Jeremy J. Baumberg, Nanoscale, 8 (2016) 15864-15869.
- [248] S. Lim, J.E. Song, J.A. La, E.C. Cho, Chem. Mater., 26 (2014) 3272-3279.
- [249] Q.Q. Liu, Y.D. Liu, Y.D. Yin, Natl. Sci. Rev., 5 (2018) 128-130.
- [250] T.H. Chow, Y. Lai, X. Cui, W. Lu, X. Zhuo, J. Wang, Small, 15 (2019) 1902608.
- [251] A. Jaiswal, L. Tian, S. Tadepalli, K.-k. Liu, M. Fei, M.E. Farrell, P.M. Pellegrino, S. Singamaneni, Small, 10 (2014) 4287-4292.
- [252] C. Li, K.L. Shuford, M. Chen, E.J. Lee, S.O. Cho, ACS Nano, 2 (2008) 1760-1769.
- [253] J. Zeng, Y. Cao, C. H. Lu, X.-d. Wang, Q. Wang, C. Y. Wen, J. B. Qu, C. Yuan, Z. F. Yan, X. Chen, Anal. Chim. Acta, 891 (2015) 269-276.

[254] J. B. Zeng, S. G. Fan, C. Y. Zhao, Q. R. Wang, T. Y. Zhou, X. Chen, Z. F. Yan, Y. P. Li, W. Xing, X. D. Wang, Chem. Commun., 50 (2014) 8121-8123.